

# Channel cross-section heterogeneity of particulate organic carbon transport in the Huanghe

Yutian Ke<sup>1†</sup>, Damien Calmels<sup>1</sup>, Julien Bouchez<sup>2</sup>, Marc Massault<sup>1</sup>, Benjamin Chetelat<sup>3</sup>, Aurélie Noret<sup>1</sup>, Hongming Cai<sup>2</sup>, Jiubin Chen<sup>3</sup>, Jérôme Gaillardet<sup>2</sup>, Cécile Quantin<sup>1</sup>

<sup>1</sup>GEOPS, Université Paris-Saclay-CNRS, 91405 Orsay, France

<sup>2</sup>Université de Paris, Institut de Physique du Globe de Paris, CNRS, 75005 Paris, France

<sup>3</sup>School of Earth System Science, Institute of Surface-Earth System Science, Tianjin University, 300072 Tianjin, China

<sup>†</sup>Present address: Division of Geological and Planetary Science, California Institute of Technology, Pasadena, CA 91125, USA

Corresponding author: Yutian KE (yutianke@caltech.edu)

**Abstract.** The Huanghe (Yellow River), one of the largest turbid river systems in the world, has long been recognized as a major contributor of suspended particulate matter (SPM) to the ocean. However, over the last few decades, the SPM export flux of the Huanghe has decreased over 90% due to the high management, impacting the global export of particulate organic carbon (POC). To better constrain sources and modes of transport of POC beyond the previously investigated transportation of POC near the channel surface, SPM samples were for the first time collected over a whole channel cross-section in the lower Huanghe. Riverine SPM samples were analyzed for particle size and major element contents, as well as for POC content and dual carbon isotopes (<sup>13</sup>C and <sup>14</sup>C). Clear vertical and lateral heterogeneities of the physical and chemical properties of SPM are observed within the river cross-section. For instance, finer SPM carry, in general more POC with higher <sup>14</sup>C activity near the surface of the right bank. Notably, we discuss how bank erosion in the alluvial plain is likely to generate lateral heterogeneity in POC composition. The Huanghe POC is millennial-aged (4,020 ± 500 radiocarbon years), dominated by organic carbon (OC) from the biosphere, while the lithospheric fraction reaches up to ca. 33%. The mobilization of aged and refractory OC, including radiocarbon-dead biospheric OC, from deeper soil horizons of the loess-paleosol sequence through erosion in the Chinese Loess Plateau is an important mechanism contributing to fluvial POC in the Huanghe drainage basin. Altogether, anthropogenic activities can drastically change the compositions and transport dynamics of fluvial POC, consequentially altering the feedback of the source-to-sink trajectory of a river system to regional and global carbon cycles.

Deleted: The results show c

Deleted: y

Deleted: SPM

Deleted: characteristics

Deleted: , with f

Deleted: example, in general,

Deleted: ing

## 36 1 Introduction

37 Rivers are the main conveyor of rock and soil debris eroded from the continents to the ocean. Along with inorganic  
38 material, river sediments host particulate organic carbon (POC) derived mainly from three major sources: 1) recently  
39 photosynthesized OC of the biosphere, 2) aged and altered OC from soils, and 3) ancient OC contained in sedimentary  
40 rocks (Blair et al., 2010). The net effect of riverine POC transport on the carbon cycle and thus on the evolution of  
41 Earth's climate depends on POC provenance and fate. The effective sedimentary burial of POC derived from the  
42 terrestrial biosphere (biospheric OC,  $OC_{bio}$ ) represents a net, long-term sink of atmospheric  $CO_2$  (Galy et al., 2007,  
43 Bouchez et al., 2014; Hilton et al., 2015), whereas the oxidation of POC derived from continental rocks (petrogenic  
44 OC,  $OC_{petro}$ ) acts as a net, long-term source of  $CO_2$  to the atmosphere (Hilton et al., 2014). The erosion and burial of  
45  $OC_{petro}$  escaping from oxidation has no net effect on the long-term carbon cycle (Galy et al., 2008a; Bouchez et al.,  
46 2010; Hilton et al., 2011; Horan et al., 2019). In addition, the reactive nature of  $OC_{bio}$  might also result in short-term  
47  $CO_2$  emission during transport from both river channels and recently-deposited sediments (Mayorga et al., 2005; Galy  
48 and Eglinton, 2011; Blair and Aller, 2012).

49 Globally, rivers transport a total POC flux of *ca.* 200 Tg C/year, consisting of  $157_{-50}^{+74}$  Tg C/year of  $OC_{bio}$  and  $43_{-25}^{+61}$   
50 Tg C/year of  $OC_{petro}$  (Galy et al., 2015; Ludwig et al., 1996). Source-to-sink processes controlling the origin and fate  
51 of riverine POC are prominently river-specific, suggesting that the impact of POC on regional and global carbon  
52 cycles might significantly vary both spatially and temporally (Blair and Aller, 2012). It is thus crucial to understand  
53 the mechanisms controlling the POC export by large rivers that integrate vast portions of the land surface, and quantify  
54 the differing sources of carbon exported by those large river systems.

55 The Huanghe (Yellow River) is a highly turbid river system that exports over 85% of its OC as particulate matter,  
56 with efficient deposition and preservation in the ocean (Cauwet and Mackenzie, 1993; Bianchi, 2011; Zhang et al.,  
57 2013; Ran et al., 2013). The Huanghe has been highly managed over the last few decades through water and soil  
58 conservation measures as well as reservoir construction, leading to a decrease of nearly 90% of its sediment load  
59 (Wang and Fu et al., 2016; Wang et al., 2007; Milliman et al., 1987) and a significant decrease in its POC delivery to  
60 the ocean (Zhang et al., 2013). Reservoir construction dramatically affects the transport and fate of both sediment load  
61 and POC in large rivers (Syvitski et al., 2005; Li et al., 2015). The estimated POC flux of the Huanghe is thought to  
62 have shifted from 4.5 Tg C/yr in the 1980s (Cauwet and Mackenzie, 1993) to 0.34-0.58 Tg C/yr nowadays (Tao et al.,  
63 2018) in response to both anthropogenic influence (Hu et al., 2015; Tao et al., 2018; Yu et al., 2019a) and natural  
64 variability of the regional hydrological cycle (Qu et al., 2020). These large-scale perturbations have likely modified  
65 the OC input from the different terrestrial pools as well as the fate of exported POC that was previously reaching  
66 deposition centers in the ocean and that now remains stuck on land. Those alterations of the carbon cycle remain to  
67 be addressed.

68 Over the last decade, POC transport in the Huanghe has been investigated for 1) determination and quantification of  
69 POC sources, based on bulk or molecular carbon isotopic composition (Tao et al., 2015; Yu et al., 2019b; Ge et al.,  
70 2020; Qu et al., 2020); 2) temporal and spatial variations in POC export and distribution among different size fractions  
71 (Ran et al., 2013; Wang 2012; 2016; Yu et al., 2019a, b; Qu et al., 2020); 3) impact of anthropogenic activities (Hu

Deleted: ,

73 et al., 2015; Tao et al., 2018; Yu et al., 2019a); and 4) burial efficiency and preservation in the ocean (Sun et al., 2018;  
74 Tao et al., 2016; Ge et al., 2020). However, all these previous studies rely on suspended sediment samples collected  
75 near the channel surface or at a single, intermediate depth in the river channel, further assuming a homogeneous  
76 distribution of suspended sediment characteristics in the water column, both vertically and laterally. It is now well  
77 recognized that suspended sediments present physical, mineralogical, chemical, and isotopic heterogeneities across  
78 river ~~transect~~ due to hydrodynamic sorting and tributary mixing (Galy et al., 2008b; Garzanti et al., 2010; Bouchez et  
79 al., 2010, 2011a). This is also true for POC, whose age and composition vary ~~following vertical water depth (e.g.,~~  
80 ~~Galy et al., 2008b; Bouchez et al., 2014; Hilton et al., 2015; Repasch et al., 2021; Schwab et al., 2022), and lateral~~  
81 ~~river transect~~ (e.g., Bouchez et al., 2014; Baronas et al., 2020), and between sediment size fractions separated in the  
82 laboratory (Yu et al., 2019b; Ge et al., 2020). Such heterogeneity warrants a re-evaluation of POC transport in the  
83 Huanghe, accounting for the variability in suspended sediment characteristics over the channel cross-section.  
84 In this study, we take advantage of in-river hydrodynamic sorting to access the full range of suspended sediment size  
85 fractions by collecting suspended particulate matter (SPM) samples along several river depth profiles distributed  
86 across a channel transect (e.g., Bouchez et al., 2014; Freymond et al., 2018; Baronas et al., 2020). We apply this  
87 sampling scheme to a cross-section of the Huanghe located 200 km upstream from the river mouth and report SPM  
88 OC content, stable isotope composition, and radiocarbon activity as well as total nitrogen, major element composition  
89 (aluminum and silicon), and particle size distribution. Based on these novel samples and data sets, this study aims at  
90 1) determining the controls on POC content in the Huanghe; 2) tracing and quantifying the sources of riverine POC  
91 in the Huanghe; and 3) providing depth-integrated estimates of POC fluxes in the most turbid large river system.

## 92 2 Study area

93 The Huanghe originates from the north-eastern Qinghai-Tibet Plateau (QTP) and runs through the Chinese Loess  
94 Plateau (CLP) and the North China Plain (NCP) to the Bohai Sea (Figure 1a). It is 5,464 km long and drains a basin  
95 area of  $79.5 \times 10^4$  km<sup>2</sup>. The Huanghe drainage basin can be subdivided into three main geomorphic units: 1) the high-  
96 relief upper reaches spanning from the source region (elevation of 4,500 m) to the city of Toudaoguai (located 3,472  
97 km downstream at an elevation of 1,000 m); 2) the middle reaches with a channel length of 1,206 km, ending at  
98 Huayuankou (elevation of 110 m) draining landscapes characterized by relatively gentle slopes; and 3) the lower  
99 reaches where the river flows eastwards across a fluvial plain over a length of 786 km. These three sections drain  
100 53.8%, 43.3%, and 2.9% of the whole Huanghe basin area, respectively (Wang et al., 2007; YRCC, 2016). Most  
101 second-order tributaries drain the CLP region and feed the main channel in the middle reaches, the Dawenhe River  
102 being the only tributary of the lower reaches, with negligible water and sediment supply due to upstream trapping in  
103 lakes and reservoirs. It is worth noting that more than 50% of the water discharge at the Huanghe's mouth comes from  
104 the QTP, whereas over 90% of the sediment load originates from the CLP (Wang et al., 2010, 2017; Pan et al., 2016).  
105 The CLP is thus the principal source area of sediment to the Huanghe (Shi and Shao, 2000; Guo et al., 2002; Wang  
106 and Fu et al., 2016).

107 The Huanghe drainage basin is mostly underlain by the North China craton, and is bounded by several mountain belts.  
108 The watershed encompasses 46% of sedimentary rock outcrops (mainly siliciclastic rocks with minor carbonates), and

Deleted: cross-sections

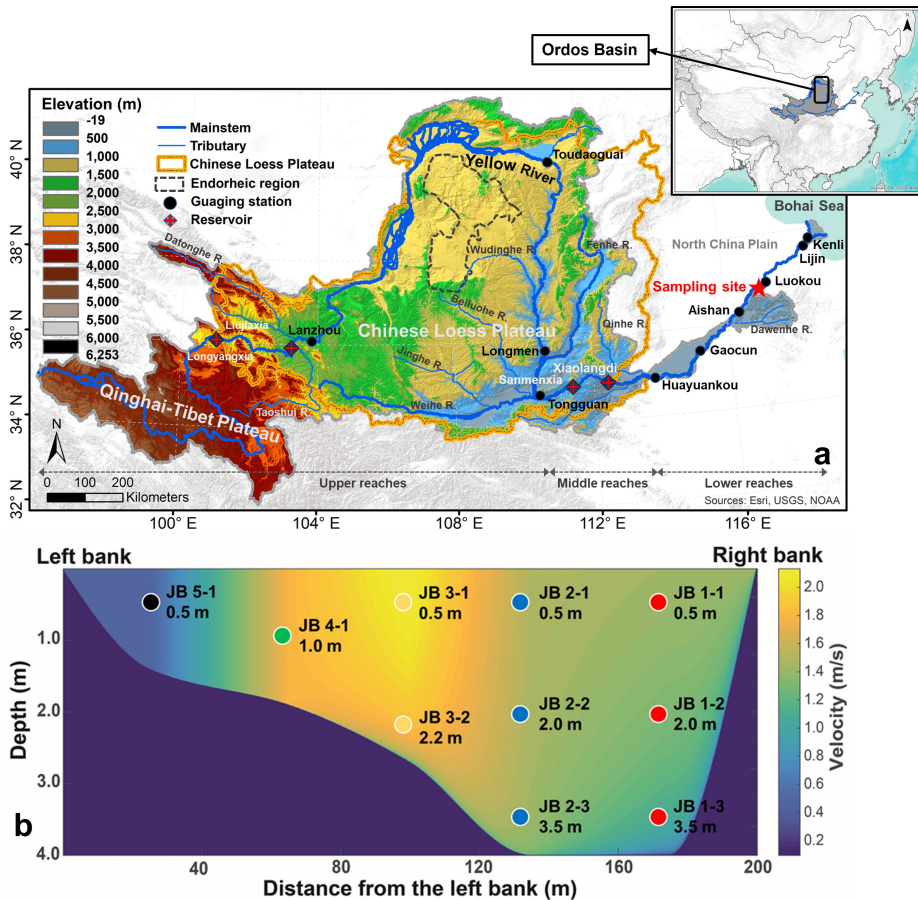
Deleted: within cross-sections

Formatted: Font: Italic

111 about 45% of unconsolidated sediments (mainly Quaternary loess deposits). The remaining outcrops include  
112 metamorphic, plutonic, and volcanic rocks formed from the Archean to the Tertiary (Figure S1). Although river  
113 incision is strong in the QTP, a substantial part of the corresponding eroded material is not effectively transferred to  
114 the lower reaches due to deposition in the CLP and the western Mu-U desert, a situation that has prevailed since at  
115 least the middle Pleistocene (Nie et al., 2015; Licht et al., 2016; Pan et al., 2016). In addition, recent anthropogenic  
116 disturbance such as constructions of large dams in the upper reaches has profoundly modified the export of solid  
117 materials from the basin (Wang et al., 2007). The Huanghe then flows through the CLP that has acted as the major  
118 supplier of sediment to the system since at least the Calabrian Pleistocene (Stevens et al., 2013; Bird et al., 2015).  
119 There, an easily erodible loess-paleosol formation has accumulated since 2.58 Ma (Guo et al., 2002), over a thickness  
120 ranging from a few meters to more than 500 m, with an average of 100 m. This loess-paleosol formation and underlying  
121 Cretaceous sedimentary rocks are actively incised by the main stem and its tributaries (Shi and Shao, 2000; Guo et  
122 al., 2002; Wang and Fu et al., 2016). Notably, the Ordos Basin underlying the CLP is rich in oil and gas (Guo et al.,  
123 2014). In the lower reaches, the river drains Quaternary fluvial deposits and sedimentary rocks.

124 The Huanghe drainage basin encompasses the entire arid and semi-arid region of northern China in the upper and  
125 middle reaches, and is characterized by more humid climate conditions in the lower reaches. Annual average  
126 precipitation (over the period 1950 - 2000) in the upper, middle and lower reaches regions is 368 mm, 530 mm, and  
127 670 mm, respectively (Wang et al., 2007). As a result of the East Asian summer and winter monsoon circulations, the  
128 rainy season (June to September) contributes 85% of the annual precipitation (Wang et al., 2007). During the rainy  
129 season, frequent storm events lead to concentrated flows (relatively high discharge) in vulnerable gully-hill systems,  
130 the dominant regional geomorphic landscape, and actively participates in soil erosion in the CLP (Shi and Shao, 2000;  
131 He et al., 2004; Qu et al., 2020). The present-day (2002 to 2016) suspended sediment flux delivered by the Huanghe  
132 to the sea is about 0.12 Gt/yr, which implies a decrease of nearly 90% in sediment export compared to the widely cited  
133 estimate of 1.08 Gt/yr (average value between 1950 to 1980, Milliman and Farnsworth, 2011). This massive decrease  
134 in sediment export mostly results from human perturbations, including soil conservation practices in the CLP and  
135 retention in large reservoirs, rather than from climatic variations such as the decreasing precipitation observed in the  
136 region over the last decades (Wang et al., 2007; Ran et al., 2013; Wang and Fu et al., 2016; [Li et al., 2022](#)). A scheme  
137 for water and sediment regulation (WSR) has been implemented through the construction of the Xiaolangdi Reservoir  
138 since 2002, aiming to mitigate water and sediment imbalances in the lower reaches. This regulation has resulted in a  
139 modification of the flux of sediment delivered to the lower reaches and estuary, making the Huanghe a highly human-  
140 regulated river system. However, no WSR was implemented in 2016, the year of our sampling campaign, suggesting  
141 that the collected SPM samples are not significantly affected by retention in dams, and thus are representative of the  
142 fluvial transport of terrestrial materials eroded from the CLP.



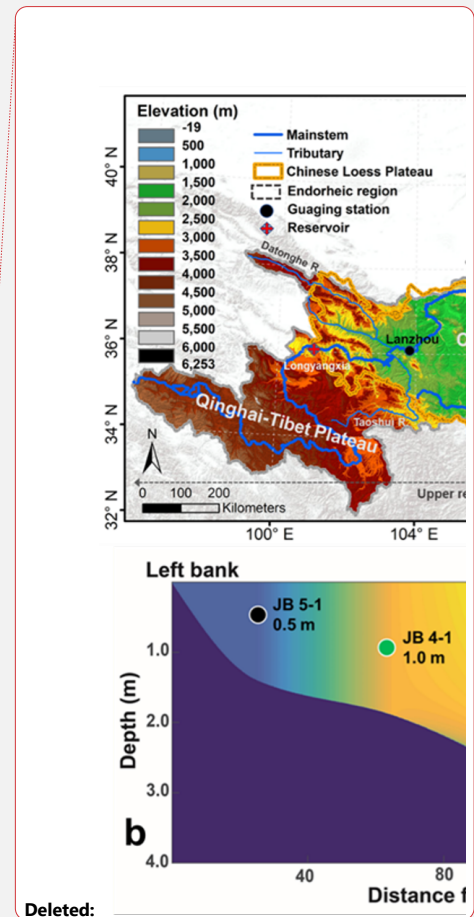


143  
 144 **Figure 1:** (a) Elevation map of the Huanghe drainage basin showing the main reservoirs and gauging stations along the  
 145 main stem as well as our sampling site (36.75°N, 117.02°E, near the Luokou gauging station); and (b) channel cross-section  
 146 sampled for this study showing the depth and lateral distribution of suspended particulate matter (SPM) samples and  
 147 modeled velocity distribution based on the "law of the wall", using the point velocity data measured by a current velocity  
 148 meter attached to the sampler.

149 **3 Sampling and analytical methods**

150 **3.1 Sampling strategy**

151 Detailed sampling of a cross-section of the Huanghe was carried out on the 17<sup>th</sup> of July, 2016, during the flood season  
 152 (Figure S2). Samples were collected along five depth profiles near the Luokou hydrological station (36.75°N, 117.02°E),  
 153 250 km upstream from the river mouth (Figure 1). This sampling strategy allows for accessing the full range of  
 154 suspended sediment particle size (Bouchez et al., 2014). The cross-section is 200-meters wide at the surface and 4



Deleted:

Formatted: Font: Not Bold

156 meters deep at most (Figure 1; [YRCC, 2016](#)). As in previous studies, we used a home-made, 10-liter, point-sediment  
157 horizontal Niskin-type sampler attached to a current velocity meter, to collect river water samples and measure the  
158 water velocity simultaneously. Subsequently, two water samples were collected at the surface near the right bank in  
159 May and June 2017 before the flooding season, to retrieve fine suspended particulate matter. For each sample,  
160 approximately 30 liters of river water were collected and were then filtered through pre-weighed 0.22- $\mu\text{m}$  porosity  
161 cellulose acetate membrane filters within 24 hours. After rinsing the filters with filtered water, all sediment samples  
162 were transferred into centrifuge tubes and freeze-dried before weighing and analysis. A bed sediment ([BS](#)) sample  
163 was collected on an exposed, recently flooded sediment bar of the riverbed.

### 164 3.2 Physical and geochemical analysis

165 Apart from a 50-mg aliquot of SPM samples preserved for particle size analysis, samples were finely ground using an  
166 agate mortar and pestle prior to chemical and isotopic analyses. The particle size distribution of the unground aliquots  
167 was measured using a Laser Diffraction Particle Size Analyzer (Beckman Coulter LS-12 320) at the École Normale  
168 Supérieure (ENS), Paris, France. Before analysis, unground SPM aliquots were dispersed in deionized water and then  
169 in sodium hexametaphosphate in an ultrasonic bath. For each sample, we measured three replicates and report the  
170 average median particle size ( $D_{50}$ ,  $\mu\text{m}$ ) with an uncertainty better than 2% (Table 1). The chemical composition of  
171 SPM samples was measured on ground aliquots at the Centre de Recherches Pétrographiques et Géochimiques  
172 (CRPG), Vandoeuvre-lès-Nancy, France, using inductively coupled plasma atomic emission spectroscopy (ICP-OES)  
173 for major elements with typical uncertainties of 3% (Carignan et al., 2001).

174 For particulate organic carbon content (POC%, wt.), stable carbon isotope  $\delta^{13}\text{C}$  (in ‰<sub>VPDB</sub>, *i.e.*, in ‰ relative to Vienna  
175 Pee Dee Belemnite) and radiocarbon isotope  $\Delta^{14}\text{C}$  (expressed as fraction modern, Fm), ground homogenized samples  
176 were fumigated using 12M HCl fumes in a closed Teflon tank at 60 °C for 48 hours to remove the carbonate fraction,  
177 and were then dried under vacuum prior to analysis. Total nitrogen content (TN%, wt.) was measured on non-acidified  
178 samples (Komada et al., 2008). Triplicate analysis on POC% and  $\delta^{13}\text{C}$  of POC (acidified aliquots) as well as TN%  
179 (non-acidified aliquots) were carried out on an Organic Elemental Analyzer (OEA) coupled with Isotope Ratio Mass  
180 Spectrometry (IRMS, Thermo Scientific Flash 2000) under continuous flow mode at Géosciences Paris Saclay  
181 (GEOPS), Orsay, France. Subjected to the blank subtraction by linearity test, two international standards including  
182 USGS-40 and IAEA-600 as well as an internal standard (GG-IPG) were used to build linear regression equations to  
183 calibrate the elemental and isotopic values for both carbon and nitrogen. Uncertainties on POC%,  $\delta^{13}\text{C}$ , and TN%,  
184 based on replicate measurements ( $1\sigma$ ,  $n=3$ ), are lower than 0.02%, 0.06‰, and 0.02‰, respectively. The  $^{14}\text{C}$  activity  
185 of POC was measured on a new compact accelerator mass spectrometry (AMS), *ECHO*MICADAS (Hatté et al., [2023](#)),  
186 using a gas ion source interface system ([GIS](#)) at the Laboratoire des Sciences du Climat et de l'Environnement (LSCE),  
187 Gif-sur-Yvette, France, with an absolute uncertainty of max  $\pm 0.5\%$ . Aside from the gas bottles of prepared blank PhA  
188 and standard NIST OX II which are permanently connected to the GIS and, used for normalization and corrections for  
189 fractionation and background, international standards including IAEA-C5, IAEA-C7, IAEA-C8, and blank PhA were  
190 prepared in different sizes (10 to 100's  $\mu\text{g C}$ ) to match the amount of OC found in the sediment samples.

Deleted: 2016

Deleted: gas in helium provided to the syringe by directly connecting gas bottles

Deleted: to do

Deleted: ,

Deleted: corrections

Deleted: untreated

Deleted: to produce from

Deleted:

Deleted: equivalent

Deleted: carbon as from

Deleted: fractions of

### 203 3.3 POC source apportionment

204 To quantify the contribution and associated uncertainties of various sources to POC transported in the Huanghe, a  
205 Bayesian Markov ~~Chain~~ Monte Carlo (MCMC) based on a three-end member (Appendix A) mixing scheme was  
206 adopted. This approach ~~considers~~ the ~~variability~~ on each end member contribution, ~~assuming this variability~~ can be  
207 represented by a normal distribution. ~~Prior information is assumed to be unknown. We computed the posterior~~  
208 ~~distribution of the Bayesian formulation using the MCMC method, facilitated by the *rjags* package ([https://cran.r-](https://cran.r-project.org/web/packages/rjags/index.html)  
209 [project.org/web/packages/rjags/index.html](https://cran.r-project.org/web/packages/rjags/index.html), Andersson et al., 2015), all computations were performed in the R  
210 environment (<http://www.r-project.org/>). To ensure reliable simulation, the model was run with 5,000,000 iterations,  
211 using a burn-in of 1000 steps, and a data thinning of 100 for each sample. The mixing model was constructed on the  
212 dual stable and radioactive isotope of the riverine POC pool ( $\delta^{13}\text{C}$  and  $\Delta^{14}\text{C}$ ) and of the three potential source pools  
213 (section 5.2) by the following equations:~~

$$\text{Isotope\_ratio}_{\text{sample}} = \sum_{\text{source}} (f_{\text{source}} * \text{Isotope\_ratio}_{\text{source}})$$
$$\sum_{\text{source}} f_{\text{source}} = 1$$

216 where  $\text{Isotope\_ratio}_{\text{sample}}$  is either the  $\delta^{13}\text{C}$  or  $\Delta^{14}\text{C}$  value of the sample,  $\text{Isotope\_ratio}_{\text{source}}$  is either the  $\delta^{13}\text{C}$  or  
217  $\Delta^{14}\text{C}$  value of different possible sources of POC and  $f_{\text{source}}$  the relative contribution of each source of POC.

### 218 3.4 Depth-integrated fluxes

219 Instantaneous depth-integrated fluxes of SPM and POC sources were calculated for the cross-section using a method  
220 developed by Bouchez et al. (2011a, b). This method is based on the systematic variation of SPM concentration in the  
221 water column (Figure 2) applying a Rouse-based model (Rouse, 1937). We first constructed a bathymetric profile of  
222 the river cross-section based on the depth information collected in the field and then modeled the velocity distribution  
223 across the transect (Figure 1b) through fits of the so-called "law of the wall" to water velocity measured at the location  
224 of each sample within the cross-section using a current meter. Afterward, the concentration of total SPM and various  
225 particle size fractions could be estimated by applying the so-called Rouse model (Rouse, 1937) to each particle size  
226 fraction separately (Bouchez et al., 2011a), resulting in a map of the particle size distribution in the river cross-section  
227 (Figure S3). The aluminum to silicon ratio (Al/Si mass ratio) is inversely related to the particle size of river SPM in  
228 the Ganges-Brahmaputra, the Amazon, and the Mackenzie Rivers (Galy et al., 2007; Bouchez et al., 2014; Hilton et  
229 al., 2015). Such a linear relationship between D50 and Al/Si was also observed in our dataset, allowing for computing  
230 the spatial distribution of POC content in the cross-section, based on the linear relationship between POC and Al/Si  
231 (Figure 3). Finally, combining modeled water velocity, SPM concentration, and POC distribution we calculated a  
232 depth-integrated, instantaneous POC flux for the whole river channel (Figure S3, detail in supplementary material).

Deleted: chain

Deleted: (burn-in of 1,000 steps, data thinning of 100, and iterations of 5,000,000)

Deleted: (Andersson et al., 2015).

Deleted: assumes that

Deleted: uncertainty

Formatted: Font: Italic

239 **4 Results**

240 We report the first isotopic dataset of POC samples collected along several depth profiles distributed over a cross-  
241 section of the Huanghe (Table 1). SPM concentrations range from 679 to 2,459 mg/L (avg. 1,286 mg/L) and show an  
242 obvious increase from the surface to the bottom and from the right bank to the left bank (Figure 1b and 2a). The  
243 surface SPM concentration (*i.e.*, samples collected 0.5 m below the surface) decreases laterally as the water column  
244 deepens. The range of measured Huanghe SPM D50, *i.e.* the median particle size (19.5-86.0  $\mu\text{m}$ , Figure 2b) agrees  
245 with that (16.6-120.1  $\mu\text{m}$ ) of SPM collected at Lijin during the same flooding season by Moodie et al. (2022). In each  
246 depth profile, SPM is consistently coarsening with depth as revealed by the evolution of grain size parameters such as  
247 D10, D50, and D90 (Table 1, Figure 2 and Figure S4). The finest SPM is transported on the right bank and at the  
248 surface, while the coarsest SPM is found at the bottom of the middle profile (sample JB 2-3). Two types of depth  
249 profiles can be distinguished at Luokou based on particle size distributions (Figure S4) and the relationship between  
250 D50 and water depth (Figure 2b). On the one hand, the JB 1 and JB 4 profiles show a well-marked, bi-modal  
251 distribution of particle size (Figure S4) together with relatively low and consistent D50 (Figure 2b). On the other hand,  
252 the JB 2, JB 3, and JB 5 profiles show a more unimodal distribution of particle size (Figure S4) and a unique D50 -  
253 sampling depth relationship (Figure 2b). Interestingly, these two groups can also be distinguished in terms of  
254 relationships between POC% and  $\delta^{13}\text{C}$  with water depth (Figures 2d and 2f). As expected, the Al/Si ratio is well-  
255 related to the particle size, and the ratios measured in the middle profile SPM samples (0.17 for JB 2-3 and 0.26 for  
256 JB 2-1) encompass the full range of Al/Si found in the whole cross-section (Figure 2c). The relatively low Al/Si ratios  
257 are comparable to that of the middle Huanghe (Qu et al., 2020) and other large turbid river systems such as the Ganges-  
258 Brahmaputra (Galy et al., 2008b), Salween, and Irrawaddy (Tipper et al., 2021).  
259 SPM in the Huanghe is characterized by low TN and POC content (wt.%), ranging from 0.04% to 0.08% ( $0.06 \pm$   
260  $0.01\%$ ) and from 0.29% to 0.42% ( $0.37 \pm 0.06\%$ ), respectively (Figure 2d; Table 1). POC content generally decreases  
261 from the surface to the river bed, with quantitative differences from one profile to another (Figure 2d). Notably, the  
262 JB 1 profile shows the highest POC% and TN%. In addition, the ratio of TN% to POC%:  $\text{N}/\text{C}_{\text{org}}$  increases with depth  
263 in the JB 1 profile (from top to bottom), while it decreases in the JB 2 and JB 3 profiles (Figure 2e). The  $\delta^{13}\text{C}$  of POC  
264 varies over a narrow range from  $-26.55\%$  to  $-25.75\%$  ( $-26.12 \pm 0.29\%$ , Figure 2f) and becomes lighter with depth,  
265 showing that fine SPM has higher  $\delta^{13}\text{C}$  than coarse SPM. These values are lower than those previously reported for  
266 other Huanghe sampling sites upstream:  $-24.7 \pm 0.4\%$  at Toudaoguai,  $-24.9 \pm 0.6\%$  at Longmen, and  $-23.8 \pm 0.6\%$   
267 at Lijin (Qu et al., 2020, Hu et al., 2015; Tao et al., 2015; Yu et al., 2019a; Ge et al., 2020). The radiocarbon activity  
268 of POC of the Huanghe at Luokou is relatively low (Figure 2g), with  $F_m$  ranging from 0.552 ( $\Delta^{14}\text{C} = -453\%$ ; sample  
269 JB2-3) to 0.675 ( $\Delta^{14}\text{C} = -331\%$ ; sample JB1-3), spanning from 3,160 to 4,780  $^{14}\text{C}$  yr, and the average value is  $0.607$   
270  $\pm 0.038$  ( $\Delta^{14}\text{C} = -412\%$ ). This range of radiocarbon activity is consistent with published values for POC collected at  
271 the river surface downstream of Toudaoguai (Qu et al., 2020). All the POC radiocarbon activity data reported so far  
272 for the Huanghe are comparable to mean values for Arctic large rivers ( $\Delta^{14}\text{C} = -397\%$ , ca. 4,480  $^{14}\text{C}$  yrs, Ke et al.,  
273 2022), revealing the multimillennial-age nature of POC transported by the Huanghe. The elemental and isotopic  
274 signatures of the two fine SPM samples HH 17.05 and HH 17.06 (on average POC% = 1.07%,  $\delta^{13}\text{C} = -25.67\%$ ,  $F_m$

Deleted: in each depth profile

Deleted: and

Deleted: is

Deleted: involving

Deleted: with

Deleted: of

Deleted: varying from 0.17 (sample JB 2-3) to 0.26 (sample JB 2-1), covering the full range of Al/Si ( $0.21 \pm 0.03$ , average with one standard deviation, herein after) measured in the whole cross-section (avg.  $0.21 \pm 0.03$ , Figure 2c).

Deleted: avg.,

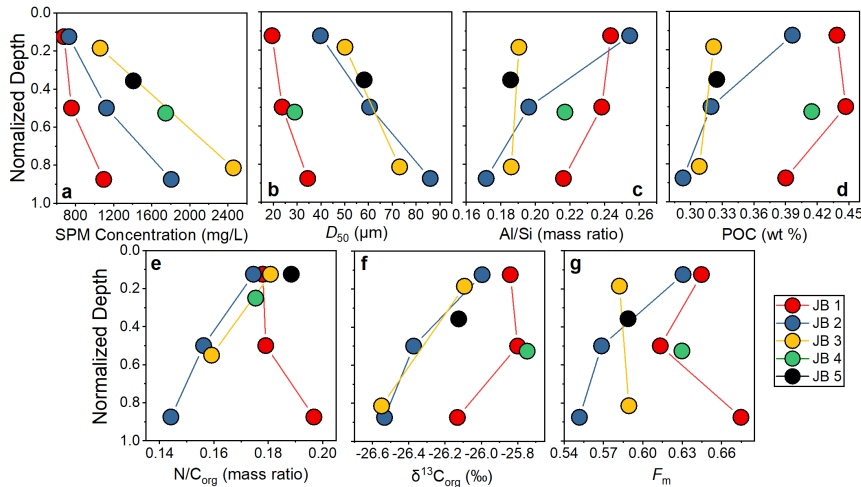
Deleted: avg.,

Deleted: avg.,

Deleted:

289 = 0.720; and Al/Si = 0.37) are significantly different from those of the depth profile samples (Table 1). The bed  
 290 sediment sample has a comparatively low POC% (0.21%),  $\delta^{13}\text{C}$  ( $-27.35\text{‰}$ ),  $F_m$  (0.099), and Al/Si ratio (0.17).

Deleted: bedload



291  
 292 **Figure 2: Variation of physical and chemical parameters in the river cross-section, shown as a function of sampling depth**  
 293 **normalized to total depth of the water column at the location of the considered depth-profile, for the Luokou cross-section**  
 294 **on the Huanghe (June 16, 2017). (a) SPM concentration; (b) particle size distribution (shown as D50); (c) Al/Si mass ratio;**  
 295 **(d) POC content (weight %); (e) N/C<sub>org</sub> mass ratio; (f) stable carbon isotope ratio  $\delta^{13}\text{C}_{\text{org}}$  (‰); (g) radiocarbon activity  $F_m$ .**

296 **Table 1: SPM characteristics and POC properties of the river-cross-section sampling.**

Sample ID	Type	Depth (m)	SPM mg/L	POC (%)	SD	$\delta^{13}\text{C}_{\text{org}}$ (‰)	SD	$F_m$	$\Delta^{14}\text{C}$ (‰)	SD	$^{14}\text{C}$ age	TN (%)	N/C <sub>org</sub>	Al/Si	D50 $\mu\text{m}$
JB 1-1	SPM	0.5	679	0.44	0.02	-25.84	0.03	0.645	-360	7	3527	0.078	0.178	0.243	19.5
JB 1-2	SPM	2	757	0.45	0.01	-25.80	0.06	0.613	-392	11	3929	0.080	0.179	0.238	23.7
JB 1-3	SPM	3.5	1095	0.39	0.01	-26.13	0.04	0.675	-331	7	3161	0.077	0.197	0.216	34.5
JB 2-1	SPM	0.5	730	0.40	0.03	-26.00	0.01	0.631	-374	7	3703	0.069	0.175	0.255	39.8
JB 2-2	SPM	2	1124	0.32	0.01	-26.37	0.06	0.569	-436	13	4537	0.050	0.156	0.196	60.4
JB 2-3	SPM	3.5	1806	0.29	0.01	-26.53	0.06	0.552	-453	38	4779	0.042	0.144	0.172	86.0
JB 3-1	SPM	0.5	1058	0.32	0.02	-26.09	0.03	0.582	-422	12	4346	0.058	0.181	0.190	50.1
JB 3-2	SPM	2.2	2459	0.31	0.02	-26.55	0.04	0.589	-415	11	4247	0.049	0.159	0.186	73.1
JB 4-1	SPM	1	1747	0.41	0.02	-25.75	0.06	0.630	-375	8	3714	0.073	0.175	0.217	29.0
JB 5-1	SPM	0.5	1406	0.32	0.01	-26.12	0.05	0.589	-416	11	4256	0.061	0.188	0.186	58.2
HH 17.05	SPM	0	83	0.92	0.00	-25.73	0.14	0.711	-295	19	2740	0.184	0.200	0.358	5.2
HH 17.06	SPM	0	54	1.21	0.01	-25.60	0.07	0.729	-277	25	2539	0.261	0.215	0.377	4.3
HH	BS			0.21	0.03	-27.35	0.05	0.099	-901	7	18539	0.019	0.087	0.175	44.4

297 **5 Discussion**

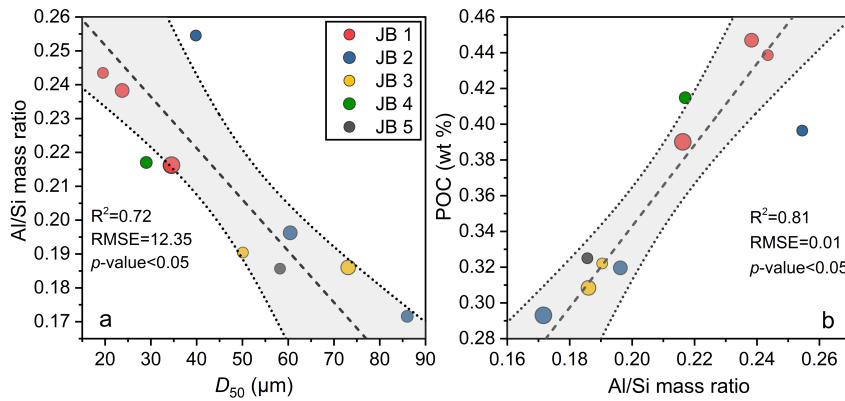
298 We observe significant heterogeneities of elemental and isotopic carbon composition as well as inorganic chemistry  
 299 over the studied river cross-section. The possible mechanisms behind these variations are assessed hereafter. Then,  
 300 sources of riverine POC are determined and quantified, confirming that erosion of the loess-paleosol sequence of the  
 301 CLP is a major source of aged and refractory biospheric OC to the Huanghe. Finally, we assess the POC load and its

303 variability over the transect profile, inferring the importance of the supply of POC from the river bottom in the  
 304 Huanghe.

### 305 5.1 Transportation mode of POC in the Huanghe

#### 306 5.1.1 POC loading and its controls

307 The Huanghe is characterized by a high SPM load with relatively low POC% ( $0.37 \pm 0.06\%$ ). In the Luokou cross-  
 308 section, POC content generally increases with decreasing particle size (Figure S5), with the two clay-sized ("HH")  
 309 samples showing the largest POC content (Table 1). Consistently, the Al/Si ratio of Huanghe sediments, which varies  
 310 as an inverse linear function of the median particle sizes  $D_{50}$  ( $R^2=0.72$ ,  $p\text{-value}<0.05$ , Figure 3a), positively correlates  
 311 with POC% ( $R^2=0.81$ ,  $p\text{-value}<0.05$ , Figure 3b), a pattern observed globally (Galy et al., 2008b; Bouchez et al., 2014;  
 312 Hilton et al., 2015; Repasch et al., 2021). This pattern is consistent with POC variability in the Huanghe reported for  
 313 manually separated size fractions of sediments (Yu et al., 2019b).

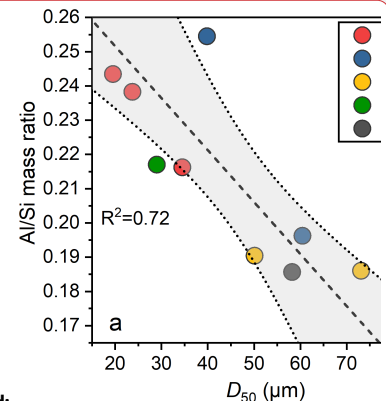


314  
 315 **Figure 3: Relationships between (a) particle size  $D_{50}$  and Al/Si mass ratio; (b) Al/Si mass ratio and POC content for the**  
 316 **Luokou cross-section on the Huanghe (July 17, 2016). *Size of circles represents water depth of the corresponding SPM.***  
 317 **The grey shade represents the 95% confidence area of the linear best-fit (black dashed line), the upper and lower bound**  
 318 **are marked by grey dotted lines.**

319 The first reason for the low POC content of Huanghe sediments is therefore their relatively low values of Al/Si  
 320 compared to other systems - a feature that can be related to the quartz-rich, OC-poor nature of the loess-paleosol  
 321 formations of the CLP (Jahn et al., 2021; Huang and Ren, 2006; He et al., 2006; Ning et al., 2006; Wang and Fu,  
 322 2016). However, Huanghe sediments are relatively poor in POC, even considering their low Al/Si, compared to other  
 323 rivers globally. To that effect, the so-called "POC loading" can be characterized by the slope described by sediment  
 324 data in an Al/Si-POC diagram (Galy et al., 2008b; Figure 4). For a given Al/Si ratio, the POC% in the Luokou cross-  
 325 section is similar to that of the middle Huanghe (Qu et al., 2020), indicating the relatively invariant transport mode of  
 326 POC between the middle and lower reaches. Previous studies have shown that the positive relationship between POC%  
 327 and Al/Si can be partially explained by OC adsorption onto the mineral surface (Curry et al., 2007; Galy et al., 2008b;  
 328 Blair and Aller, 2012; Bouchez et al., 2014; Qu et al., 2020). In the loess-paleosol deposits acting as a source of

Deleted: avg.

Formatted: Font: Italic



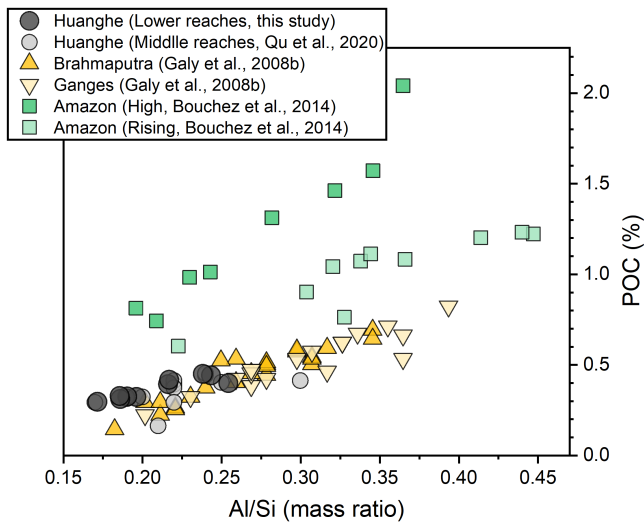
Deleted:

Formatted: Centered



331 sediments to the Huanghe, OC is mostly preserved and stabilized by forming organo-aggregates with kaolinite and  
 332 through adsorption onto iron oxides (Wang et al., 2013).  
 333 However, POC loading in the Huanghe is small compared to that of the Amazon (Bouchez et al., 2014), but similar  
 334 to that of the Ganges-Brahmaputra system (Galy et al., 2008b). While many factors could influence POC loading  
 335 across these catchments, we note that another similarity between the Huanghe and Ganges-Brahmaputra fluvial  
 336 systems is their millennial-aged OC<sub>bio</sub> (Galy et al., 2007; Tao et al., 2016). This is in stark contrast with the Amazon,  
 337 where younger OC<sub>bio</sub> ages have been reported (Bouchez et al., 2014). Given that younger OC<sub>bio</sub> recently  
 338 photosynthesized in terrestrial or aquatic ecosystems can be readily oxidized within catchments (Mayorga et al., 2005),  
 339 the relatively low POC loading observed at the mouth of the Ganges-Brahmaputra and the Huanghe (Figure 4) could  
 340 be related to the predominance of refractory, aged OC<sub>bio</sub> and OC<sub>petro</sub> in those systems, while the Amazon sediments  
 341 would still contain significant amount of younger, more labile OC<sub>bio</sub>.

Deleted: refractory



342  
 343 **Figure 4: "POC loading" of river SPM of large rivers. The POC loading is estimated from the slope of the relationship**  
 344 **between POC content and the Al/Si ratio of each fluvial system (Galy et al., 2008b). All SPM samples were collected along**  
 345 **depth profiles except for the middle Huanghe (Qu et al., 2020).**

346 In detail, and as explained in more detail below (Section 5.1.2) we also observe a significantly different POC loading  
 347 between the JB 1 and JB 2 depth profiles at the Luokou station (Figure 3). This difference in POC loading in the cross-  
 348 section of the Huanghe might indicate the delivery of recent OC<sub>bio</sub>, specifically near the right bank (the closest to the  
 349 JB 1 profile) for the Luokou site, a scenario which is supported by the comparatively younger age of POC in profile  
 350 JB 1. Consistently with this interpretation, temporally variable POC loading at a given site has been reported for the  
 351 Amazon (Bouchez et al., 2014), where higher POC loading during the high-water stage compared to the rising water  
 352 stage has been attributed to the erosion of discrete organic debris from riverbanks.

353 Variable POC loading amongst large catchments has implications for evaluating the likelihood of POC preservation  
 354 in estuaries. The Ganges-Brahmaputra system delivers relatively old, refractory OC<sub>bio</sub> to the Bengal Fan with an almost

356 complete burial efficiency (Galy et al., 2007). Given the observed similarity in POC loading and age, we can thus  
357 expect a similar, efficient preservation for the Huanghe offshore depositional system. In addition to the low reactivity  
358 of the POC transported by the Huanghe, the high sediment accumulation rates in the Huanghe coastal domain might  
359 further inhibit OC oxidation (Blair and Aller, 2012). Consequently, the case of the Huanghe differs drastically from  
360 that of the Amazon, where higher POC loading is observed, with a larger contribution of young, labile OC<sub>bio</sub> either as  
361 discrete organic matter or associated with mineral surfaces, leading to low POC burial efficiency in the ocean  
362 (Bouchez et al., 2014; Blair and Aller, 2012).

### 363 5.1.2 Chemical heterogeneity within the transect

364 There is clear lateral and vertical variability of POC content and SPM inorganic chemistry across the Luokou cross-  
365 section of the Huanghe. For each vertical depth profile, clay-rich fine particles are transported near the channel surface,  
366 and quartz-rich coarse particles flow near the river bottom. Accordingly, the Al/Si ratio, POC content and POC  
367 radiocarbon activity generally decrease with depth. Elemental (POC%) and isotopic POC signatures (<sup>13</sup>C and <sup>14</sup>C) are  
368 inversely related to the particle size (D50; Figure S5). These patterns are observed in other large fluvial systems, e.g.,  
369 Ganges and Brahmaputra, Amazon and Mackenzie (Galy et al., 2008b; Bouchez et al., 2014, Hilton et al., 2015),  
370 showing that hydrodynamic sorting is the primary control on suspended sediment OC content, segregating inorganic  
371 and organic material according to particle size (Bouchez et al., 2011a, 2014).

372 At the Luokou sampling site, lateral variability at the channel surface shows that POC-rich fine particles are  
373 preferentially transported near the right bank (Figure 2 and Figure S3). This pattern is validated by the Rouse model  
374 provided in Text S1, the Rouse number ( $Z_R$ ) is 0.137, 0.236, and 0.284 for JB-1, JB-2, and JB-3, respectively. In  
375 essence, the Rouse number ( $Z_R$ ) can reflect the balance between gravitation settling and upward turbulent diffusion.  
376  $Z_R$  is smaller near the right bank while larger near the left bank, showing heterogeneity across the transect. Larger  
377 particles exhibit a faster settling velocity due to their increased weight, leading to a higher  $Z_R$ . On the other hand, the  
378 lighter ones settle more slowly, resulting in  $Z_R$  approaching 0. This means that their concentration remains relatively  
379 consistent throughout varying depths. However, as depth increases and the concentration of larger particles grows, the  
380 proportion of these finer particles in the overall sediment decreases (Bouchez et al., 2011a). The channel geometry  
381 thus needs to be examined as a potential factor to produce such lateral heterogeneity, in particular the mechanisms of  
382 bed sediment resuspension and bank erosion.

383 Resuspension of bed sediments is also a possible mechanism that could explain the lateral heterogeneity in POC  
384 content in the study cross-section of the Huanghe. Indeed, scouring of channel bed sediment at high water flow may  
385 also shift POC to more negative radiocarbon and stable isotope signatures. Our sample set collected in July 2016  
386 during a flooding period (water flow velocity up to 2.1 m/s, Figure 1) supports this scenario. Indeed, the increase in  
387 D50 of surface SPM samples from right to the left bank, that is with total channel depth decrease, is consistent with  
388 coarse sediment resuspension from the bed. This is also supported by the Rouse model, where higher  $Z_R$  in the shallow  
389 water near the left bank indicates a greater likelihood of sediment settling to the bed. Lower  $Z_R$  suggests that there is  
390 enhanced SPM supply from the riverbed. Such a scenario is also supported by the three-fold increase in SPM flux

**Deleted:** The channel geometry thus needs to be examined as a potential factor to produce such lateral heterogeneity, in particular through bank erosion and bedload resuspension.

**Deleted:** o

**Formatted:** Font: Italic

**Formatted:** Subscript

**Deleted:** p

**Deleted:** being

**Deleted:** ,

**Deleted:** that approach

**Commented [DC1]:** Constant ??

**Commented [DC2]:** Along a given depth profile??

**Deleted:** through

**Moved (insertion) [1]**

**Deleted:** R

**Deleted:** to

**Deleted:** why

**Deleted:** the

**Formatted:** Font: Italic

**Deleted:** the

**Formatted:** Font: Italic

**Deleted:** sediment

**Deleted:** to suspension

**Deleted:** In addition, s

**Deleted:** S

**Deleted:** sediment

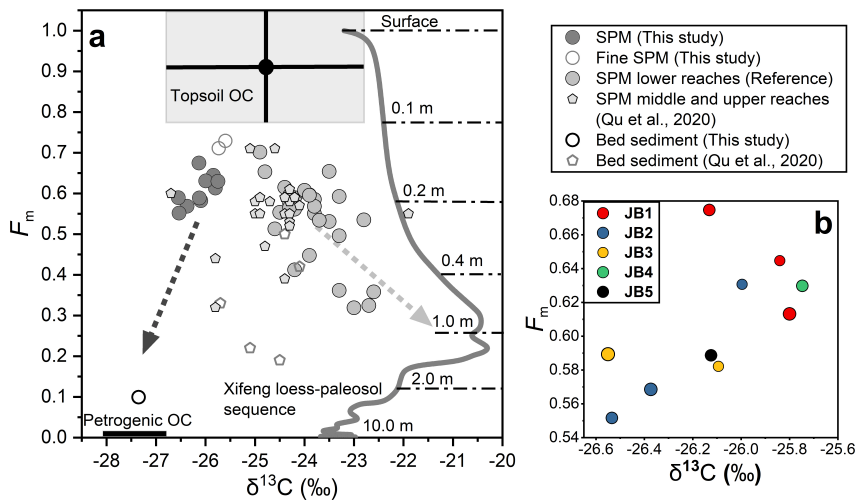


410 observed from the upstream Huayuankou station to the downstream Lijin station in July 2016, despite a four-fold  
 411 decrease in water discharge (Figure S2).  
 412 Bank erosion can be a significant mechanism for the delivery of sediments to river systems (Guo et al, 2007). Bank  
 413 erosion at Luokou would make OC from the lower Huanghe alluvial plain a potential source of POC in the lower  
 414 reaches of the Huanghe. Frequent inundation to the adjacent riparian zones in flooding seasons, surface runoff driven  
 415 by storm events, and agriculture irrigation etc., can mobilize young soil OC and discrete organic matter debris (e.g.,  
 416 plant-derived debris) to riverine POC (Hilton et al., 2011; Turowski et al., 2016). This mechanism provides a possible  
 417 explanation for the opposite trends displayed by samples from the JB 1 and JB 2 profiles in the Fm vs.  $\delta^{13}\text{C}$  space  
 418 (Figure 5). The youngest POC was found at the bottom of the JB 1 profile (JB 1-3). Meanwhile, the JB 1 samples have  
 419 comparatively higher N/C<sub>org</sub> ratios and N%, consistent with the input of discrete plant-derived debris from the bank  
 420 in addition to rock-derived detrital clastic material in the coarse fractions (> 32  $\mu\text{m}$ , Yu et al., 2019b). The transport  
 421 and entrainment of plant debris deep in the water column has been evidenced in many large river systems, such as the  
 422 Amazon (Feng et al., 2016), the Ganges-Brahmaputra (Lee et al., 2019), the Mackenzie (Schwab et al., 2022), the Rio  
 423 Bermejo River (Repasch et al., 2021). Such input would also provide an explanation for the higher POC loading of  
 424 the JB 1 profile (Section 5.1.1).

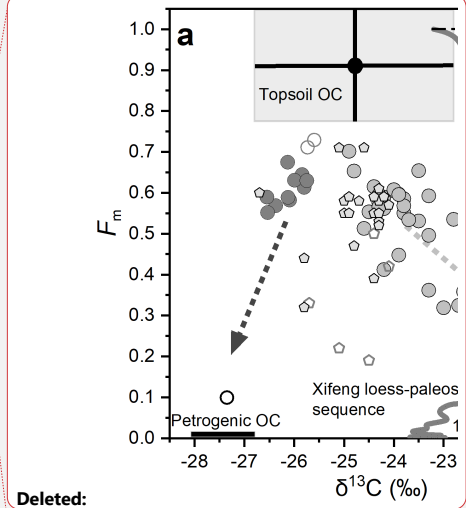
Deleted: along the course of the Huanghe  
 Deleted: ¶

Deleted: organic matter  
 Deleted: (e.g., plant debris)  
 Deleted: in  
 Deleted: s  
 Deleted: is  
 Deleted: s  
 Deleted: for example,

**Moved up [1]:** Resuspension of bed sediments is also a possible mechanism to explain the lateral heterogeneity in POC content in the study cross-section of the Huanghe. Indeed, scouring of channel bed sediment at high water flow may also shift POC to more negative radiocarbon and stable isotope signatures. Our sample set collected in July 2016 during flooding (water flow velocity up to 2.1 m/s, Figure 1) supports this scenario. Indeed, the increase in D50 of surface SPM samples from right to the left bank, that is with total channel depth decrease, is consistent with coarse sediment resuspension from the bed. Such a scenario is also supported by the three-fold increase in sediment flux observed along the course of the Huanghe from Huayuankou to Lijin in July 2016, despite a four-fold decrease in water discharge (Figure S2).¶



425 Figure 5: (a)  $^{14}\text{C}$  activity (expressed as Fm) vs.  $\delta^{13}\text{C}$  for a compilation of POC data collected over the 2011-2016 period in  
 426 the lower Huanghe, including samples from this study and previous studies at Huayuankou, Lijin, and Kenli (Hu et al.,  
 427 2015; Tao et al., 2015; Yu et al., 2019a; and Ge et al., 2020); SPM and bed sediment (BS) collected by Qu et al., 2020 at  
 428 Toudaoguai (most downstream location of the upper reaches) and Longmen in the middle reaches (Table S1). The grey  
 429 curve corresponds to  $\delta^{13}\text{C}_{\text{org}}$  of the top 10 m of the Xifeng loess-paleosol (Ning et al., 2006), and the corresponding Fm was  
 430 calculated from  $^{10}\text{Be}$ -derived ages following 'Age =  $-8033 \cdot \ln(\text{Fm})$ '. The soil depth is marked above the dot-dash line (Zhou  
 431 et al., 2010). Topsoil OC represents OC from the upper 10 cm of the loess-paleosol sequence with standard deviation marked  
 432



Deleted:  
 Formatted: Centered  
 Deleted: bedload

459 with black lines. (b)  $^{14}\text{C}$  activity (expressed as Fm) vs.  $\delta^{13}\text{C}$  diagram for the Huanghe sediment samples collected in this  
460 study at the Luokou cross-section. Size of circles represents water depth of the corresponding SPM.

## 461 5.2 POC provenance in the Huanghe: the significance of loess-paleosol-derived OC

### 462 5.2.1 Physical erosion of the loess-paleosol sequence

463 Over decennial to centennial time scales, the POC export of the Huanghe is mainly controlled by erosion of the CLP.  
464 Throughout the Quaternary, the erosion rate in the Huanghe basin has been mainly driven by climate shifts until human  
465 activities started and profoundly impacted sediment fluxes in the mid-Holocene (He et al., 2006). The Huanghe has  
466 experienced a 90% decrease in annual sediment load since the 1950s (Wang et al., 2015), caused by weakened soil  
467 erosion to the CLP and sediment retention by dams (Wang et al., 2007; Ran et al., 2013; Wang and Fu et al., 2016; Li  
468 et al., 2022). To determine the contributions of the various terrestrial OC components to Huanghe POC, we compiled  
469 published POC carbon isotope data for sediments collected in the lower reaches from 2011 to 2016, after the  
470 Xiaolangdi Reservoir was operated (Figures 5 and 6). This dataset shows that the radiocarbon ages of Huanghe POC  
471 are considerably old ( $5,100 \pm 1,700$   $^{14}\text{C}$  yr,  $n=29$ ), with a minor fraction of modern photosynthesized  $\text{OC}_{\text{bio}}$  (Tao et  
472 al., 2015; Yu et al., 2019a, b). This relatively  $^{14}\text{C}$ -depleted POC suggests the significant contribution of OC originated  
473 from deep soil horizons within the catchment. Given that loess is easily erodible and that there is widespread gully  
474 erosion in the catchment, more intensive erosion of the CLP can mobilize more soils as well as older OC from deep  
475 soil horizons to fluvial transport. Therefore, higher sediment load in the river can be characterized by radiocarbon-  
476 depleted POC. This is evidenced by the negative trend between  $^{13}\text{C}$  and Fm of POC for sediment samples collected in  
477 the Huanghe over the 2011-2016 period (Figure 5a), suggesting that deep horizons of the loess-paleosol formations  
478 are a plausible source for the  $^{14}\text{C}$ -depleted end member. Besides, the preferential erosion of bomb carbon affected,  
479 recently photosynthesized and possibly degraded  $\text{OC}_{\text{bio}}$  from the overlying topsoils (< 10 cm) most likely contributes  
480 to riverine POC (Tao et al., 2015).

481 As such, variable contribution of aged and radiocarbon-free OC from deep horizons of loess-paleosol formations of  
482 the CLP should have a significant impact on the elemental and isotopic signature of POC in the lower Huanghe.  
483 Erosion of loess-paleosol can also explain the decreasing POC% with increasing SPM concentration at different sites  
484 of the main channel (Ran et al., 2013; Qu et al., 2020), the negative relationship between SPM concentration and  
485 corresponding POC Fm at Luokou ( $R^2=0.47$ ,  $p\text{-value}<0.05$ , Figure 6), and the low POC loading of the Huanghe  
486 (section 5.1.1), as the deep horizons of the loess-paleosol sequences are OC-poor, and mostly host OC that is highly  
487 degraded and refractory (Liu et al., 2012; Wang et al., 2013; Cheng et al., 2020). However, the slight increase of POC  
488  $\delta^{13}\text{C}$  with increasing SPM concentration ( $R^2=0.26$ ,  $p\text{-value}<0.05$ ,) might indicate a significant supply of soil OC from  
489 loess-paleosol shallower depth, as inferred from the  $\delta^{13}\text{C}$  variation within the Xifeng loess-paleosol sequence (Figure  
490 5a).

Deleted: before

Deleted: Even though the Huanghe has experienced a 90% decrease in annual sediment load since the 1950s (Wang et al., 2015), t

Deleted: avg

Deleted: the fact

Deleted: higher and

Deleted: to

Deleted: er

Deleted: , thus

Deleted: have

Deleted: more

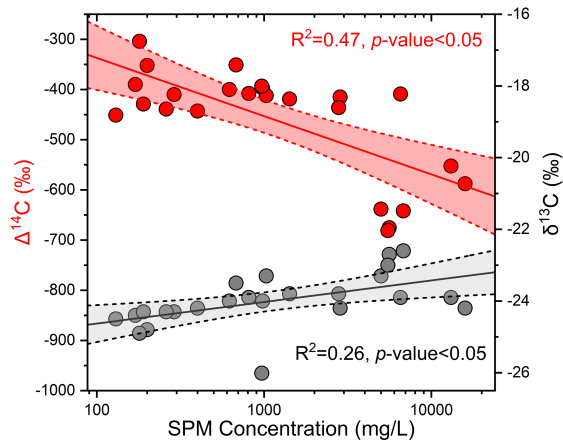
Deleted: depleted

Deleted: signals in

Deleted: Given the fact that loess is easily erodible, t

Deleted: suggests

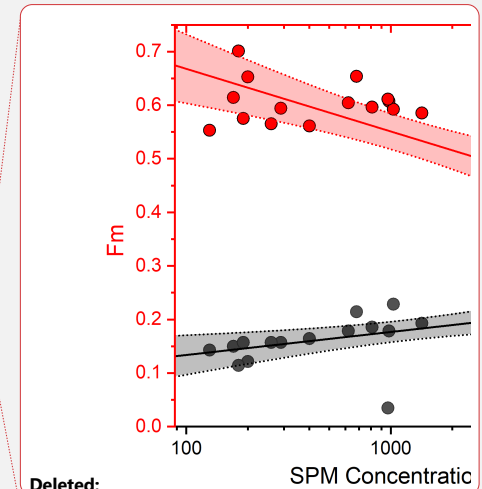
Formatted: Superscript



507  
508 **Figure 6:**  $^{14}\text{C}$  activity (expressed as Fm; red circles) and  $\delta^{13}\text{C}$  (grey circles) of POC vs. SPM concentration for surface  
509 samples from the Huanghe collected from 2011 to 2016 (average SPM concentration of surface samples in this study and  
510 from Hu et al. (2015), Tao et al. (2015), Yu et al. (2019a), and Ge et al. (2020)). These paired dual carbon isotope data  
511 corresponds to the group 'SPM lower reaches' in Figure 5. Straight lines correspond to best-fit logarithmic curves, and  
512 shaded areas represent the 95% confidence interval.

513 The  $\text{N}/\text{C}_{\text{org}}$  ratio provides additional evidence for the significant contribution of loess-paleosol material to Huanghe  
514 POC (Figure S6). Indeed, the  $\text{N}/\text{C}_{\text{org}}$  ratios of SPM collected in the lower reaches ranges from 0.10 to 0.23 (this study,  
515 Ran et al., 2013; Yu et al., 2019a), whereas topsoils of the CLP are characterized by  $\text{N}/\text{C}_{\text{org}}$  lower than 0.14 (Liu and  
516 Liu, 2017) and sedimentary rocks typically have very low  $\text{N}/\text{C}_{\text{org}}$  (Hilton et al., 2015). Soil OC input from the North  
517 China Plain is also unlikely given its  $\text{N}/\text{C}_{\text{org}}$  of 0.10-0.13 (Shi et al., 2017). Therefore, all these possible sources cannot  
518 explain the high  $\text{N}/\text{C}_{\text{org}}$  signatures of riverine SPM. In addition, the high turbidity of the Huanghe ( $> 600 \text{ mg/L}$ ) during  
519 the sampling season is likely to inhibit *in-situ* primary production ( $\text{N}/\text{C}_{\text{org}} > 0.13$ ) (Zhang et al., 2013; Hu et al., 2015).  
520 As a result, only soil OC from deep loess-paleosol horizons appears as a plausible supplier to downstream Huanghe  
521 POC, given the high  $\text{N}/\text{C}_{\text{org}}$  ratios previously reported for various loess-paleosol sequences (Figure S6, Ning et al.,  
522 2006).

523 Geomorphic processes in the CLP region support the erosion of deep soil horizons. There, gully erosion is thought to  
524 be responsible for more than 80% of the total sediment yield in the CLP (He et al., 2006; Li et al., 2022). Gullies are  
525 densely distributed and cover about 42% of the total area of the CLP and up to 60% in hilly regions (Huang and Ren,  
526 2006; He et al., 2006). Nowadays, the well-developed gully geomorphic system of the CLP is characterized by gullies  
527 with a depth of about 10 m on average and represents the most active vertical and regressive erosion of loess (Huang  
528 and Ren, 2006). This incision process erodes all types of unconsolidated materials, including the loess-paleosol  
529 sequence, underlying red clays, and colluvial deposits in the form of creeps, falls, and slides in the watershed (Zhu,  
530 2012). From 1925 to 1981, the erosion rate of the CLP was  $6,317.9 \text{ t km}^{-2} \text{ yr}^{-1}$ , compared to  $10,770 \text{ t km}^{-2} \text{ yr}^{-1}$  in the  
531 hilly and gully plateau (Li et al., 2022). While the CLP's erosion rate dropped to  $3,475.9 \text{ t km}^{-2} \text{ yr}^{-1}$  between 1982 and  
532 2016, the rate in the hilly and gully plateau remained significantly high at  $6,146.5 \text{ t km}^{-2} \text{ yr}^{-1}$  (Li et al., 2022). All these  
533 observations suggest that gully erosion can strongly impact the composition of riverine POC. As gully erosion is



Deleted:

Formatted: Centered

Deleted: black

Deleted: s

537 sensitive to climate change and anthropogenic activities, soil dynamics in the Huanghe basin have been altered since  
 538 the mid-Holocene (He et al., 2006; Li et al., 2022). Notably, the strengthening of the East Asian Monsoon in coming  
 539 decades (Li et al., 2022; Xue et al., 2023) could potentially enhance this process. However, in recent years, soil and  
 540 water conservation and environmental rehabilitation campaigns (Wang et al., 2007) largely contributed to the  
 541 reduction of SPM export by the Huanghe with a transfer to the estuary of 10.6 Mt in 2016, which is one order of  
 542 magnitude lower than the annual sediment flux measured in 2013 (172.8 Mt) and two orders or magnitude lower  
 543 compared to the flux of the 1950s (ca. 1,340 Mt; Wang et al., 2015). This sediment load reduction is consistent with  
 544 the weakened erosion rate observed in the CLP, such modifications should thus have drastically inhibited the OC  
 545 mobilization from the CLP and the POC export by the Huanghe.

Deleted: In

Deleted: represents a few percent of

Deleted: less than one percent of the

Deleted: Such

### 546 5.2.2 POC source determination and end member apportionment

547 Considering the SPM geochemistry and the basin characteristics, three terrestrial sources can be identified as necessary  
 548 to form the composition of the Huanghe POC at the Luokou cross-section. As discussed in Section 5.2.1 and shown  
 549 in Figure 5a, two of these sources are (a) topsoil-derived OC ( $OC_{ts}$ ) and (b) OC from deeper horizons of the loess-  
 550 paleosol sequence ( $OC_{lps}$ ) excluding topsoil. In addition, at the Luokou cross-section, bed OC shows lower  $F_m$  and  
 551  $\delta^{13}C$  values compared to that of SPM, suggesting a significant contribution of (c) rock-derived OC from erosion in the  
 552 middle reaches ( $OC_{petro}$ ).

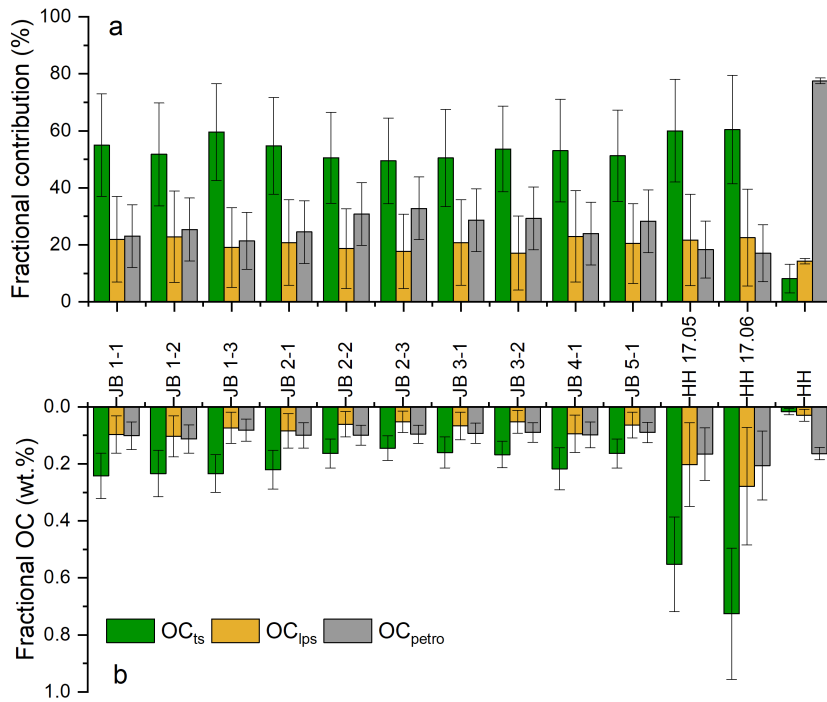
553 We adopted a Bayesian Monte-Carlo model to reconstruct source apportionment based on the mass balance of carbon  
 554 isotopes ( $\delta^{13}C$  and  $\Delta^{14}C$ ) of our three defined end members (section 3.3, Table 2, Appendix A). Modeling results are  
 555 shown in Figure 7 as relative contributions (Figure 7a) and weight percentage (Figure 7b) of  $OC_{ts}$ ,  $OC_{lps}$ , and  $OC_{petro}$   
 556 (Table S2). The contribution of  $OC_{petro}$  to total Huanghe POC at Luokou varies between 21% and 33% in the cross-  
 557 section, which is higher than the contribution calculated for in the two fine SPM samples (17% on average) and much  
 558 smaller than for the bed sediment sample ( $78 \pm 10\%$ ). The inferred  $OC_{petro}$  concentration in the sediment is remarkably  
 559 uniform in the cross-section, representing  $0.10 \pm 0.01\%$  of SPM (Figure 7b). This result is consistent with the OC  
 560 contents of midstream sedimentary rocks at  $0.09 \pm 0.08\%$  (Qu et al., 2020). In addition, these findings imply that  
 561  $OC_{petro}$  concentration does not depend on particle size and confirm previous findings of  $OC_{petro}$  being present in a  
 562 range of clastic particles or as discrete particles (Galy et al., 2008a; Bouchez et al., 2014). In other words, the rock-  
 563 derived OC has a relatively invariant contribution with depth (Galy et al., 2008a; Bouchez et al., 2014), meaning that  
 564 biospheric OC exerts a first-order control on POC content and isotopic variations throughout the cross-section.

565 **Table 2: Summary of  $\delta^{13}C$  and  $\Delta^{14}C$  of source end members for POC in the Huanghe.**

End member	$\delta^{13}C$	$\Delta^{14}C$
$OC_{ts}$	$-24.8 \pm 1.9\text{‰}$	$-90 \pm 130\text{‰}$
$OC_{lps}$	$-22.7 \pm 1.0\text{‰}$	$-610 \pm 390\text{‰}$
$OC_{petro}$	$-29.2 \pm 0.9\text{‰}$	$-1000\text{‰}$

566 At the study cross-section,  $OC_{ts}$  and  $OC_{lps}$  contribute 50%-60% and 17%-23% to the total POC, respectively (Figure  
 567 7a). The sum of these two components can be considered as  $OC_{bio}$ , which varies between 67% and 77%. The  
 568 corresponding  $OC_{bio}$  content of sediment is quite variable, ranging from 0.20% (sample JB 2-3) to 0.34% (sample JB  
 569 1-1), and generally decreases from the river surface to the bottom. Given the rather invariant  $OC_{petro}$  concentration in

574 the sediment, there are thus marked heterogeneities of POC provenance in the cross-section. For instance, POC  
 575 transported close to the right bank and in the finer SPM samples show a higher contribution from OC<sub>bio</sub>. From the  
 576 knowledge of the relative contributions of OC<sub>ts</sub> and OC<sub>lps</sub> and their corresponding <sup>14</sup>C activity, the Fm values for the  
 577 bulk OC<sub>bio</sub> can be estimated based on mass balance. The modeled radiocarbon activity of OC<sub>bio</sub> is relatively  
 578 homogeneous with an average Δ<sup>14</sup>C value of -178 ± 11‰ (1,510 ± 110 <sup>14</sup>C yr) whereas a greater variance is observed  
 579 in the bulk <sup>14</sup>C content. In summary, our results support the first-order control of OC<sub>bio</sub> abundance on POC content  
 580 and age in the Huanghe.



581 **Figure 7: (a) Relative contributions of the three different sources of Huanghe POC, (b) fractional OC weight percentage**  
 582 **Huanghe POC at the Luokou cross-section, as inferred from a mixing model. OC<sub>ts</sub> is the topsoil-derived OC, OC<sub>lps</sub>**  
 583 **represents the loess-paleosol sequence OC excluding topsoil, and OC<sub>petro</sub> is the rock-derived OC eroded from the Huanghe**  
 584 **middle reaches.**

586 Applying the same mixing model to previously published Huanghe POC data (2011-2016, Table S1) shows (1)  
 587 dominance of the OC<sub>bio</sub> contribution to POC, (2) variable relative mixing proportions of OC<sub>ts</sub> and OC<sub>lps</sub>; (3) a wide  
 588 range of <sup>14</sup>C age for OC<sub>bio</sub> (from 1,040 to 8,050 yr). In particular, OC<sub>ts</sub> and OC<sub>lps</sub> contributed 20%-30% and 46%-68%  
 589 to POC collected in 2013 (Hu et al., 2015), leading to 75-89% of OC<sub>bio</sub>. Yu et al. (2019a) estimated that OC<sub>bio</sub>  
 590 contributed 63%-81% to the lower Huanghe POC (2015-2016) using a different mixing model. Using their data in our  
 591 mixing model results in a slightly higher OC<sub>bio</sub> contribution of 77%-87%, consisting of 39%-53% for OC<sub>ts</sub> and 30%-  
 592 47% for OC<sub>lps</sub>. The small difference in source contribution mainly results from the fact that old OC<sub>bio</sub> from loess-

593 paleosol sequences was not considered in Yu et al. (2019a), and from the different isotopic signatures chosen for the  
594 POC endmembers. However, both estimates ignore the possible presence of rock-derived OC in soils. In any case, our  
595 results suggest that the Huanghe transports more OC<sub>bio</sub>-derived POC than previously thought, with more aged, soil-  
596 derived OC.

597 It is worth noticing that these calculations suggest that the OC<sub>lps</sub> fraction in the Huanghe was significantly higher in  
598 2013 than in 2016. As most Huanghe sediments are derived from the CLP, higher physical erosion in the CLP should  
599 enhance supply of aged, refractory OC<sub>bio</sub> to the river system. ~~Consequently~~, the decrease in sediment supply from the  
600 CLP initiated a few decades ago (Wang and Fu et al., 2016), which is likely to continue in the future, will probably  
601 lead to the reduction of the contribution of OC<sub>lps</sub> to total POC export from the Huanghe. This might have an impact  
602 on the burial efficiency of riverine POC on the continental margins, as OC<sub>ls</sub> is more labile than OC<sub>lps</sub>, and thus more  
603 prone to the remineralization process before burial. Moreover, decreasing erosion rate in the Huanghe basin will lead  
604 to decreasing sediment accumulation rate in the estuary, which potentially favors the oxidation of all POC components  
605 before burial (Blair and Aller, 2012). The time scale over which such effect could take place is yet unknown, as  
606 anthropogenic intervention is the primary reason for the sediment yield reduction, through afforestation and soil and  
607 water conservation measures in the CLP and reservoir operation in the middle reaches of the Huanghe. However, it is  
608 plausible that in response to decreased terrestrial physical erosion on the Loess Plateau over at least decadal timescales,  
609 an increased proportion of Huanghe POC will be oxidized before burial in the ocean, thereby leading to a weakened  
610 preservation efficiency for the terrestrial eroded POC.

Deleted: As a consequence

### 611 5.3 POC export by the Huanghe

612 In the Huanghe, POC content varies both vertically and laterally throughout the cross-section (Figure 2). This spatial  
613 variability of both physical and chemical SPM characteristics must be considered when estimating integrated  
614 instantaneous POC concentration and flux (Section 3.4).

615 We calculate that (Text S1) at the sampling time (July 2016), the Huanghe at Luokou transported 1,075 kg/s of SPM  
616 for a water discharge of 731 m<sup>3</sup>/s, such that the spatially-integrated SPM concentration over the cross section (SPM<sub>int</sub>)  
617 was 1,472 mg/L, a value relatively close to the straightforward average concentration of our 10 samples (1,286 mg/L).  
618 The Luokou gauging station records a monthly SPM load of 1,826 kg/s in July 2016, and the daily average SPM load  
619 of 1,096 kg/s for a daily average water discharge of 643 m<sup>3</sup>/s on the 16<sup>th</sup> and 17<sup>th</sup> of July 2016 (method: three water  
620 samples collected at 0.5 m below the channel surface across the transect profile, data available at  
621 <http://www.yrcc.gov.cn>). Even though the latter estimate neglects the vertical heterogeneity within this relatively  
622 shallow river (< 5.0 m), estimates give similar results.

623 We further obtain an instantaneous POC flux of 3.69 kg/s, corresponding to a cross-section integrated average POC  
624 content (POC<sub>int</sub>%) of 0.34% when dividing this instantaneous POC flux by the instantaneous SPM load. Given the  
625 relatively homogenous distribution of OC<sub>petro</sub>, the instantaneous flux of OC<sub>petro</sub> was calculated by multiplying the  
626 average OC<sub>petro</sub> content by the instantaneous cross-section integrated SPM flux, yielding 1.07 ± 0.11 kg/s. The  
627 instantaneous OC<sub>bio</sub> flux was then calculated by subtracting the instantaneous flux of OC<sub>petro</sub> from the instantaneous  
628 POC flux, yielding 2.61 ± 0.26 kg/s. Assuming that our SPM samples are representative in terms of POC content

630 exported in July 2016, and taking the SPM flux of the gauging station for July, then the estimated fluxes of POC,  
631 OC<sub>bio</sub>, and OC<sub>petro</sub> for the flood period of July 2016 are 6.1, 4.3, and 1.8 kg/s, respectively. Taking POC<sub>int</sub> content for  
632 estimating the annual POC flux yields a value of 1.1 kg/s consisting of 0.8 and 0.3 kg/s for OC<sub>bio</sub> and OC<sub>petro</sub> fluxes,  
633 respectively. Note that these numbers are lower-bound estimates because POC content in Huanghe SPM collected  
634 during flood periods is generally the lowest (Ran et al., 2013). [Taking the highest POC content 0.75% reported in the](#)  
635 [lower Huanghe in 2016 \(Yu et al., 2019a\), the estimated annual POC flux is 2.4 kg/s.](#)

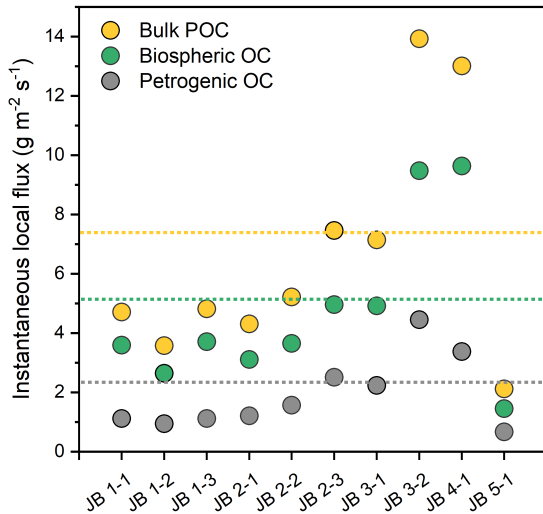
636 The above numbers present a sharp decrease compared to the estimated POC and OC<sub>bio</sub> fluxes transported by the  
637 Huanghe over the period 2008 to 2013. Galy et al. (2015) estimated an OC<sub>petro</sub> flux of 1.9 kg/s and an OC<sub>bio</sub> flux of  
638 11.4 kg/s from 2008 to 2012 (SPM flux: 3,655 kg/s, YRCC 2016), while Tao et al. (2018) reported an OC<sub>petro</sub> flux of  
639 5.8 kg/s and a similar OC<sub>bio</sub> flux of 12.6 kg/s from June 2012 to May 2013 (SPM flux: 5,723 kg/s, YRCC 2016).

640 We first note that previous estimates of POC flux in the Huanghe might be biased as these estimates neglect the  
641 variability over the cross-section (*e.g.*, Hu et al., 2015; Ran et al., 2013; Tao et al., 2015), SPM samples analyzed so  
642 far for the Huanghe were generally collected within the first 0.5 m below the surface, meaning that previous POC  
643 estimates did not consider the observed vertical and lateral POC heterogeneities and have thus misestimated POC  
644 sources and fluxes. Those estimates were calculated by multiplying an individual surface POC content by the  
645 corresponding monthly or weekly suspended sediment load, as provided by hydrological stations. Such estimates can  
646 be problematic because POC content in SPM generally decreases from top to bottom (Figure 2), resulting in biased  
647 surface-based estimates of fluxes (Bouchez et al., 2014). Using our cross-section data, we can estimate the bias in  
648 POC flux estimates when a single sample is used for such flux estimates, by multiplying depth-integrated sediment  
649 flux by the POC content of each sample. Such calculation shows different POC fluxes ranging from -15% to +30%  
650 compared to the depth-integrated estimate, which is mostly influenced by the variable POC content. Considering SPM  
651 collected at the channel surface, POC flux estimates using samples JB 1-1 and JB 2-1 are 28% and 15% higher,  
652 respectively, and are 6% and 5% lower using samples JB 3-1 and JB 5-1, respectively, than the depth-integrated  
653 estimate. This simple sensitivity analysis shows that channel surface sampling of SPM alone does not necessarily  
654 result in an overestimation of POC flux because of lateral heterogeneity, even though the POC content of SPM is  
655 generally higher at the surface than at the bottom (Figure 2). As a consequence, and although accurate estimation of  
656 POC fluxes requires grain-size variations to be accounted for, the corresponding bias cannot explain the large  
657 difference between our estimates of Huanghe POC export for the year 2016 and previous estimates for preceding  
658 years. [The SPM flux is 336 kg/s in 2016 and 762 kg/s over the period 2014 to 2016, which is one order of magnitude](#)  
659 [lower than values reported from 2008 to 2013 \(YRCC 2016\).](#) The dramatic decrease in sediment load of the Huanghe

660 (Wang and Fu et al., 2016) has most likely exerted a first-order control on the reduction in POC export from the  
661 Huanghe river system, and will probably continue to do so in the near future.

662 In the lower Huanghe, the POC content is very low and has small variance among different size fractions (Get et al.,  
663 2020), such that the POC flux is controlled by the SPM flux. In particular, it is worth noting that the Huanghe displays  
664 strong density stratification effects compared to other rivers (Moodie et al., 2022), with near-bed flow dominating the  
665 transport of SPM. In order to appraise how spatial and temporal variability in SPM flux could influence POC export,  
666 "local" POC loads can be calculated throughout the cross-section using the local water velocity, SPM concentration,

667 and POC content (Figure 8). In general, in the lower Huanghe more POC is transported near the riverbed and above  
 668 shallower bathymetry on the left side of the channel (except for profile JB 5). For instance, there is a nearly two-fold  
 669 increase in POC export from the surface to the bottom for the JB 2 and JB 3 profiles. The maximum local bulk POC  
 670 export (sample JB 3-2),  $OC_{bio}$  (sample JB 3-2), and  $OC_{petro}$  (sample JB 4-1) are over 6 times higher than the  
 671 corresponding minimum values (sample JB 5-1). This spatial pattern of POC load is almost the reverse of the POC%  
 672 variation over the cross-section, again stressing the importance of sediment river dynamics in POC delivery. From  
 673 these considerations, it could be anticipated that during the low-water season, when water velocity is slower, near-  
 674 bottom Huanghe SPM is deposited on the channel bed, withdrawing a significant fraction of the POC export, as shown  
 675 in other large rivers (Ke et al., 2022). This topic should be further examined in future research, in order to  
 676 systematically investigate the stratification of sediment and associated OC transport dynamics in lowland and high-  
 677 turbidity fluvial systems.



679  
 680 **Figure 8: Estimates of instantaneous “local” fluxes of Huanghe bulk POC,  $OC_{bio}$  and  $OC_{petro}$ , calculated for each sample of**  
 681 **the Luokou cross-section. The three dotted lines marked in orange, green, and grey represent the corresponding**  
 682 **instantaneous, cross-section integrated fluxes.**

683 Interestingly, anthropogenic activities may have antagonistic effects on POC export. Deforestation, agriculture, and  
 684 mining have considerably enhanced the sediment yield from the CLP since the mid-Holocene (He et al., 2006) while  
 685 the construction of large dams, soil and water conservation measures, and afforestation has considerably reduced the  
 686 sediment yield since the 1950s (Wang and Fu et al., 2016; Wang et al., 2007; Syvitski et al., 2005). Yet the Huanghe  
 687 exports substantial  $OC_{bio}$  and  $OC_{petro}$  with a significantly higher burial efficiency (~42% on average; Sun et al., 2018)  
 688 than other large fluvial systems entering passive continental margins, such as the Changjiang, Amazon, and  
 689 Mississippi (Blair and Aller, 2012). It is reported that aged soil OC is nearly fully preserved in continental margins  
 690 and that  $OC_{petro}$  has a *ca.* 70% burial efficiency (Tao et al., 2016). However, the contribution of the Huanghe OC burial



691 to the global C sink is likely to be lower in the future as the consequence of 1) sharp decrease in SPM and POC export  
692 due to weakened physical erosion in the CLP; 2) reduced sediment accumulation rate favoring OC remineralization  
693 in estuaries (Blair and Aller, 2012; Walling and Fan, 2003; Milliman and Farnsworth, 2011; Galy et al., 2015).

## 694 **6 Conclusions**

695 In this contribution, we present the first detailed study of particulate organic carbon (POC) over a complete river cross-  
696 section of the Huanghe, providing new perspectives on the transport mode, source, and instantaneous fluxes of POC  
697 in this highly turbid large river.

698 At the scale of a cross-section, physical and chemical properties of SPM are heterogeneous both vertically and  
699 laterally, a feature that is mainly controlled by bathymetry and hydrodynamic sorting. Resuspension of bed sediment  
700 and local erosion of the right bank together impact the suspended POC composition at the sampled location. This  
701 spatial heterogeneity shows that near-bottom SPM plays a dominant role in the delivery of OC<sub>bio</sub> (topsoil and deep  
702 soil OC combined) and OC<sub>petro</sub>. Despite a relatively shallow river channel (< 5.0 m) and narrow width (< 200 m), we  
703 show how the heterogeneity of POC transport over a cross-section needs to be considered in constraining POC  
704 transport mode and estimating POC fluxes.

705 Despite its millennial age, POC in the Huanghe is dominated by OC<sub>bio</sub> with a contribution of from 67% to 79%. OC<sub>petro</sub>  
706 content in SPM is relatively homogeneous (0.08% - 0.11%) over the cross-section, indicating that the variability in  
707 bulk POC age is mainly controlled by the variability in OC<sub>bio</sub> content, especially in the finest SPM fraction. OC<sub>bio</sub> ages  
708 deduced from the application of a mixing model to previously published data (record period 2011-2016) are highly  
709 variable, ranging from 1,040 to 8,050 <sup>14</sup>C yr. We interpret this feature as resulting from the erosion of deep horizons  
710 by gully systems in the loess-paleosol sequences containing <sup>14</sup>C-dead OC<sub>bio</sub>. Enhanced erosion of deep loess-paleosol  
711 horizons mobilizes aged and refractory OC to the ocean, with high burial efficiency on the passive margin. The erosion  
712 of loess-paleosol horizons is thus an efficient process of CO<sub>2</sub> burial. However, the construction of large dams has  
713 drastically affected the sediment load of the Huanghe system and retains substantial quantities of sediments that were  
714 previously exported to the ocean. Future work is needed to further quantify how these anthropogenic modifications  
715 alter POC composition and transport, by conducting comprehensive cross-section sampling campaigns over extended  
716 time series upstream and downstream from dams.

## 717 **Appendix A**

718 Fluvial POC delivered in the Huanghe POC could originate from three terrestrial sources (Table. 2). As topsoil  
719 typically contains recently photosynthesized OC<sub>bio</sub>, we used a  $\delta^{13}\text{C}$  value of  $-24.8 \pm 1.9\text{‰}$  (n=166) according to the  
720 subsurface soil OC values measured across the Huanghe basin (Rao et al., 2017). Over the sampled cross-section, the  
721 depleted <sup>13</sup>C values indicate the dominant and almost exclusive input of C3 plant-derived material to the Huanghe  
722 POC in the lower reaches. Based on <sup>14</sup>C (Liu et al., 2012) and <sup>10</sup>Be (Zhou et al., 2010) dating of < 10 cm-deep soil  
723 horizons in the Huanghe Basin, the average age of topsoil was chosen as being younger than 2,000 yr (*i.e.*,  $\Delta^{14}\text{C} >$   
724  $-220\text{‰}$ ). As the topsoil end member includes modern biospheric material ( $\Delta^{14}\text{C}$  around 40‰, Hua et al., 2013), we

725 assigned a  $\Delta^{14}\text{C}$  value of  $-90 \pm 130\text{‰}$  ( $F_m = 0.91 \pm 0.13$ ) to this endmember. This range also includes the range of  
726  $\Delta^{14}\text{C}$  values of pre-aged soil OC indicated by the long-chain  $n\text{-C}_{24+26+28}$  alkanols of the Huanghe POC reported by Tao  
727 et al. (2015) and Yu et al. (2019a). Their results show consistent POC  $\Delta^{14}\text{C}$  values in the lower reaches of  $-204 \pm$   
728  $20\text{‰}$  ( $F_m = 0.80 \pm 0.03$ ,  $n=7$ ) from June 2015 to May 2016 and  $-219 \pm 33\text{‰}$  ( $F_m = 0.79 \pm 0.04$ ,  $n=4$ ) at Kenli and of  
729  $-198 \pm 15\text{‰}$  ( $F_m = 0.81 \pm 0.02$ ,  $n=6$ ) from June 2015 to April 2016 at Huayuankou.

730 The second end member should be characterized by aged and refractory OC from the loess-paleosol sequence  
731 excluding topsoil (upper 10 m) of the CLP. Radiocarbon dating has an upper age limit of around 50,000 yr, age above  
732 which  $F_m$  is equal to 0. However, radiocarbon-free OC spanning from 50,000 to 100,000 yr must still be considered  
733 as  $\text{OC}_{\text{bio}}$  in the long-term carbon cycle. Here, we name this ignored OC as the “dormant” OC, without which the  $\text{OC}_{\text{bio}}$   
734 (*i.e.*, less than 100,000 yr old) would be underestimated to some extent because the radiocarbon-free OC would be  
735 misinterpreted as having a petrogenic origin. To consider this “dormant” OC, a  $\delta^{13}\text{C}$  values of  $-22.7 \pm 1.0\text{‰}$  and a  
736  $\Delta^{14}\text{C}$  values of  $-610 \pm 390\text{‰}$  ( $F_m$ ,  $0.39 \pm 0.39$ ) were adopted based on an average of values over the whole loess-  
737 paleosol sequence. Although radiocarbon-free (*i.e.*, older than 100,000 yr) OC overlaps with this endmember, such  
738 old soil organic carbon is probably not mobilized as modern gully erosion mainly concerns the upper 10 m of the  
739 loess-paleosol sequences, where soil  $\text{OC}_{\text{bio}}$  is assumed to be significantly younger comparatively (Figure 5).

740 Rock-derived OC from the QTP and the CLP, as well as kerogen from oil-gas fields from the Ordos Basin,  
741 were all considered to be possible contributors to the  $\text{OC}_{\text{petro}}$  endmember. The  $\delta^{13}\text{C}$  of  $\text{OC}_{\text{petro}}$  greatly varies between  
742 the QTP ( $-21.2 \pm 1.2\text{‰}$ ,  $n=11$ , Liu et al., 2007) and the CLP ( $-26.8 \pm 0.5\text{‰}$ ,  $n=8$ , Qu et al., 2020). However, most of  
743 the sediments eroded from the QTP are not transferred to the lower reaches as they remain trapped in the CLP and the  
744 western Mu Us desert (Nie et al., 2015; Licht et al., 2016; Pan et al., 2016). In addition, the construction of large dams  
745 in the upper reaches has considerably reduced the transfer of solid materials downstream (Wang et al., 2007).  
746 Therefore, rock-derived OC inherited from the denudation of the QTP region is not further considered. Kerogen from  
747 the oil-gas fields of the Ordos Basin in the CLP region (Figure 1) has  $\delta^{13}\text{C}$  values of  $-29.2 \pm 0.9\text{‰}$  ( $n=10$ , Guo et al.,  
748 2014). Taking these constraints together, we consider a  $\delta^{13}\text{C}$  value of  $-28.1 \pm 1.5\text{‰}$  for the  $\text{OC}_{\text{petro}}$  end member, and  
749 a  $\Delta^{14}\text{C}$  value of  $-1000\text{‰}$  ( $F_m = 0$ ) by definition.

## 750 Key Points

- 751 • Bank erosion in lower Huanghe provides recent organic carbon to fluvial transport, altering the particulate  
752 organic carbon transport over a river channel cross-section;
- 753 • Erosion of deep soil horizons of the loess-paleosol sequence contributes radiocarbon-dead organic carbon  
754 from the biosphere to the Huanghe;
- 755 • Channel-bottom transport in the Huanghe is the primary process of exporting fluvial particulate organic  
756 carbon to the estuary.

## 757 Data availability

758 All datasets are included in the paper and the supplementary materials.

759 **Author contributions**

760 DC, JB, CQ, and YK conceptualized the study. DC, JB, YK, MM, and BC determined the methodology. HC and JC  
761 collected the sediment samples. YK, MM, and AN assisted with elemental and isotopic carbon analysis. DC and CQ  
762 supervised the work. KY performed data analysis and wrote the original draft, and all authors contributed to the review  
763 and editing of the paper.

764 **Competing interests**

765 We declare there is no competing interest.

766 **Acknowledgments**

767 We thank Yulong Liu and Shengliu Yuan for their help during sampling and filtering. We also thank François Thil  
768 and Nadine Tissenerat for invaluable help when running the ECHOMICADAS, and Pierre Barré for use of the  
769 Beckman Coulter's LS 13 320 for particle size analysis at École normale supérieure.

770 **Financial support**

771 This study was financially supported by the Agence Nationale de la Recherche (ANR) SEDIMAN (Grant ANR-15-  
772 CE01-0012), the National Natural Science Foundation of China (NSFC), grants 41561134017, 41625012, and the  
773 China Scholarship Council (CSC) to Yutian Ke (No.201706180008).

774 **References**

- 775 Andersson, A., Deng, J., Du, K., Zheng, M., Yan, C., Sköld, M., and Gustafsson, Ö.: Regionally-Varying Combustion  
776 Sources of the January 2013 Severe Haze Events over Eastern China, *Environ. Sci. Technol.*, 49, 2038–2043,  
777 <https://doi.org/10.1021/es503855e>, 2015.
- 778 Baronas, J. J., Stevenson, E. I., Hackney, C. R., Darby, S. E., Bickle, M. J., Hilton, R. G., Larkin, C. S., Parsons, D.  
779 R., Myo Khaing, A., and Tipper, E. T.: Integrating Suspended Sediment Flux in Large Alluvial River Channels:  
780 Application of a Synoptic Rouse-Based Model to the Irrawaddy and Salween Rivers, *Journal of Geophysical Research:*  
781 *Earth Surface*, 125, <https://doi.org/10.1029/2020jf005554>, 2020.
- 782 Bianchi, T. S.: The role of terrestrially derived organic carbon in the coastal ocean: A changing paradigm and the  
783 priming effect, *Proceedings of the National Academy of Sciences*, 108, 19473–19481,  
784 <https://doi.org/10.1073/pnas.1017982108>, 2011.
- 785 Bird, A., Stevens, T., Rittner, M., Vermeesch, P., Carter, A., Andô, S., Garzanti, E., Lu, H., Nie, J., Zeng, L., Zhang,  
786 H., and Xu, Z.: Quaternary dust source variation across the Chinese Loess Plateau, *Palaeogeography,*  
787 *Palaeoclimatology, Palaeoecology*, 435, 254–264, <https://doi.org/10.1016/j.palaeo.2015.06.024>, 2015.
- 788 Blair, N. E. and Aller, R. C.: The Fate of Terrestrial Organic Carbon in the Marine Environment, *Annual Review of*  
789 *Marine Science*, 4, 401–423, <https://doi.org/10.1146/annurev-marine-120709-142717>, 2012.
- 790 Blair, N. E., Leithold, E. L., Brackley, H., Trustrum, N., Page, M., and Childress, L.: Terrestrial sources and export of  
791 particulate organic carbon in the Waipaoa sedimentary system: Problems, progress and processes, *Marine Geology*,  
792 270, 108–118, <https://doi.org/10.1016/j.margeo.2009.10.016>, 2010.
- 793 Bouchez, J., Galy, V., Hilton, R. G., Gaillardet, J., Moreira-Turcq, P., Pérez, M. A., France-Lanord, C., and Maurice,  
794 L.: Source, transport and fluxes of Amazon River particulate organic carbon: Insights from river sediment depth-  
795 profiles, *Geochimica et Cosmochimica Acta*, 133, 280–298, <https://doi.org/10.1016/j.gca.2014.02.032>, 2014.

796 Bouchez, J., Gaillardet, J., France-Lanord, C., Maurice, L., and Dutra-Maia, P.: Grain size control of river suspended  
797 sediment geochemistry: Clues from Amazon River depth profiles, *Geochemistry, Geophysics, Geosystems*, 12, n/a/  
798 n/a, <https://doi.org/10.1029/2010gc003380>, 2011a.

799 Bouchez, J., Lupker, M., Gaillardet, J., France-Lanord, C., and Maurice, L.: How important is it to integrate riverine  
800 suspended sediment chemical composition with depth? Clues from Amazon River depth-profiles, *Geochimica et*  
801 *Cosmochimica Acta*, 75, 6955–6970, <https://doi.org/10.1016/j.gca.2011.08.038>, 2011.

802 Carignan, J., Hild, P., Mevelle, G., Morel, J., and Yeghicheyan, D.: Routine Analyses of Trace Elements in Geological  
803 Samples using Flow Injection and Low Pressure On-Line Liquid Chromatography Coupled to ICP-MS: A Study of  
804 Geochemical Reference Materials BR, DR-N, UB-N, AN-G and GH, *Geostandards Newsletter*, 25, 187–198,  
805 <https://doi.org/10.1111/j.1751-908X.2001.tb00595.x>, 2001.

806 Cauwet, G. and Mackenzie, F. T.: Carbon inputs and distribution in estuaries of turbid rivers: the Yang Tze and Yellow  
807 rivers (China), *Marine Chemistry*, 43, 235–246, [https://doi.org/10.1016/0304-4203\(93\)90229-h](https://doi.org/10.1016/0304-4203(93)90229-h), 1993.

808 Cheng, P., Burr, G. S., Zhou, W., Chen, N., Hou, Y., Du, H., Fu, Y., and Lu, X.: The deficiency of organic matter 14C  
809 dating in Chinese Loess-paleosol sample, *Quaternary Geochronology*, 56, 101051,  
810 <https://doi.org/10.1016/j.quageo.2019.101051>, 2020.

811 Curry, K. J., Bennett, R. H., Mayer, L. M., Curry, A., Abril, M., Biesiot, P. M., and Hulbert, M. H.: Direct visualization  
812 of clay microfabric signatures driving organic matter preservation in fine-grained sediment, *Geochimica et*  
813 *Cosmochimica Acta*, 71, 1709–1720, <https://doi.org/10.1016/j.gca.2007.01.009>, 2007.

814 Dellinger, M., Gaillardet, J., Bouchez, J., Calmels, D., Galy, V., Hilton, R. G., Louvat, P., and France-Lanord, C.:  
815 Lithium isotopes in large rivers reveal the cannibalistic nature of modern continental weathering and erosion, *Earth*  
816 *and Planetary Science Letters*, 401, 359–372, <https://doi.org/10.1016/j.epsl.2014.05.061>, 2014.

817 [Feng, X., Feakins, S. J., Liu, Z., Ponton, C., Wang, R. Z., Karkabi, E., Galy, V., Berelson, W. M., Nottingham, A.](https://doi.org/10.1002/2016JG003323)  
818 [T., Meir, P., and West, A. J.: Source to sink: Evolution of lignin composition in the Madre de Dios River system](https://doi.org/10.1002/2016JG003323)  
819 [with connection to the Amazon basin and offshore, \*Journal of Geophysical Research: Biogeosciences\*, 121, 1316–](https://doi.org/10.1002/2016JG003323)  
820 [1338, <https://doi.org/10.1002/2016JG003323>, 2016.](https://doi.org/10.1002/2016JG003323)

821 Freymond, C. V., Lupker, M., Peterse, F., Haghipour, N., Wacker, L., Filip, F., Giosan, L., and Eglinton, T. I.:  
822 Constraining Instantaneous Fluxes and Integrated Compositions of Fluvially Discharged Organic Matter, *Geochem*  
823 *Geophys Geosy*, 19, 2453–2462, <https://doi.org/10.1029/2018gc007539>, 2018.

824 Gaillardet, J., Dupré, B., Louvat, P., and Allègre, C. J.: Global silicate weathering and CO<sub>2</sub> consumption rates deduced  
825 from the chemistry of large rivers, *Chemical Geology*, 159, 3–30, [https://doi.org/10.1016/s0009-2541\(99\)00031-5](https://doi.org/10.1016/s0009-2541(99)00031-5),  
826 1999.

827 Galy, V. and Eglinton, T.: Protracted storage of biospheric carbon in the Ganges–Brahmaputra basin, *Nature Geosci*,  
828 4, 843–847, <https://doi.org/10.1038/ngeo1293>, 2011.

829 Galy, V., Beyssac, O., France-Lanord, C., and Eglinton, T.: Recycling of graphite during Himalayan erosion: a  
830 geological stabilization of carbon in the crust, *Science*, 322, 943–5, <https://doi.org/10.1126/science.1161408>, 2008a.

831 Galy, V., France-Lanord, C., and Lartiges, B.: Loading and fate of particulate organic carbon from the Himalaya to  
832 the Ganga–Brahmaputra delta, *Geochimica et Cosmochimica Acta*, 72, 1767–1787,  
833 <https://doi.org/10.1016/j.gca.2008.01.027>, 2008b.

834 Galy, V., France-Lanord, C., Beyssac, O., Faure, P., Kudrass, H., and Palhol, F.: Efficient organic carbon burial in the  
835 Bengal fan sustained by the Himalayan erosional system, *Nature*, 450, 407–10, <https://doi.org/10.1038/nature06273>,  
836 2007.

837 Galy, V., Peucker-Ehrenbrink, B., and Eglinton, T.: Global carbon export from the terrestrial biosphere controlled by  
838 erosion, *Nature*, 521, 204–7, <https://doi.org/10.1038/nature14400>, 2015.

839 Garzanti, E., Andò, S., France-Lanord, C., Vezzoli, G., Censi, P., Galy, V., and Najman, Y.: Mineralogical and  
840 chemical variability of fluvial sediments: 1. Bedload sand (Ganga–Brahmaputra, Bangladesh), *Earth and Planetary*  
841 *Science Letters*, 299, 368–381, <https://doi.org/10.1016/j.epsl.2010.09.017>, 2010.

842 Garcia, M.: *Sedimentation Engineering*, American Society of Civil Engineers, (pp. 21-163)  
843 <https://doi.org/10.1061/9780784408148>, 2008.

844 Ge, T., Xue, Y., Jiang, X., Zou, L., and Wang, X.: Sources and radiocarbon ages of organic carbon in different grain  
845 size fractions of Yellow River-transported particles and coastal sediments, *Chemical Geology*, 534, 119452,  
846 <https://doi.org/10.1016/j.chemgeo.2019.119452>, 2020.

847 Gu, Z., Duan, X., Shi, Y., Li, Y., and Pan, X.: Spatiotemporal variation in vegetation coverage and its response to  
848 climatic factors in the Red River Basin, China, *Ecological Indicators*, 93, 54–64,  
849 <https://doi.org/10.1016/j.ecolind.2018.04.033>, 2018.

Formatted: Left, Pattern: Clear

Formatted: Font color: Auto, English (US)

850 Guo, H., Jia, W., Peng, P., Lei, Y., Luo, X., Cheng, M., Wang, X., Zhang, L., and Jiang, C.: The composition and its  
851 impact on the methane sorption of lacustrine shales from the Upper Triassic Yanchang Formation, Ordos Basin, China,  
852 *Marine and Petroleum Geology*, 57, 509–520, <https://doi.org/10.1016/j.marpetgeo.2014.05.010>, 2014.

853 Guo, K., Zou, T., Jiang, D., Tang, C., and Zhang, H.: Variability of Yellow River turbid plume detected with satellite  
854 remote sensing during water-sediment regulation, *Continental Shelf Research*, 135, 74–85,  
855 <https://doi.org/10.1016/j.csr.2017.01.017>, 2017.

856 Guo, L., Ping, C.-L., and Macdonald, R. W.: Mobilization pathways of organic carbon from permafrost to arctic rivers  
857 in a changing climate, *Geophysical Research Letters*, 34, <https://doi.org/10.1029/2007GL030689>, 2007.

858 Guo, Z. T., Ruddiman, W. F., Hao, Q. Z., Wu, H. B., Qiao, Y. S., Zhu, R. X., Peng, S. Z., Wei, J. J., Yuan, B. Y., and  
859 Liu, T. S.: Onset of Asian desertification by 22 Myr ago inferred from loess deposits in China, *Nature*, 416, 159–163,  
860 <https://doi.org/10.1038/416159a>, 2002.

861 [Hatté, C., Arnold, M., Dapoigny, A., Daux, V., Delibrias, G., Boisgucheneuc, D. D., Fontugne, M., Gauthier, C.,  
862 Guillier, M.-T., Jacob, J., Jaudon, M., Kaltnecker, É., Labeyrie, J., Noury, C., Paterne, M., Pierre, M., Phouybanhdyt,  
863 B., Poupeau, J.-J., Tannau, J.-F., Thil, F., Tisnérat-Laborde, N., and Valladas, H.: Radiocarbon dating on  
864 ECHOMICADAS, LSCE, Gif-Sur-Yvette, France: new and updated chemical procedures, \*Radiocarbon\*, 1–16,  
865 <https://doi.org/10.1017/RDC.2023.46>, 2023.](https://doi.org/10.1017/RDC.2023.46)

866 He, X., Zhou, J., Zhang, X., and Tang, K.: Soil erosion response to climatic change and human activity during the  
867 Quaternary on the Loess Plateau, China, *Reg Environ Change*, 6, 62–70, <https://doi.org/10.1007/s10113-005-0004-7>,  
868 2006.

869 Hemingway, J. D., Hilton, R. G., Hovius, N., Eglinton, T. I., Haghipour, N., Wacker, L., Chen, M. C., and Galy, V.  
870 V.: Microbial oxidation of lithospheric organic carbon in rapidly eroding tropical mountain soils, *Science*, 360, 209–  
871 212, <https://doi.org/10.1126/science.aao6463>, 2018.

872 Hemingway, J. D., Rothman, D. H., Grant, K. E., Rosengard, S. Z., Eglinton, T. I., Derry, L. A., and Galy, V. V.:  
873 Mineral protection regulates long-term global preservation of natural organic carbon, *Nature*, 570, 228–231,  
874 <https://doi.org/10.1038/s41586-019-1280-6>, 2019.

875 Hilton, R. G., Gaillardet, J., Calmels, D., and Bircch, J.-L.: Geological respiration of a mountain belt revealed by the  
876 trace element rhenium, *Earth and Planetary Science Letters*, 403, 27–36, <https://doi.org/10.1016/j.epsl.2014.06.021>,  
877 2014.

878 Hilton, R. G., Galy, A., Hovius, N., Horng, M.-J., and Chen, H.: Efficient transport of fossil organic carbon to the  
879 ocean by steep mountain rivers: An orogenic carbon sequestration mechanism, *Geology*, 39, 71–74,  
880 <https://doi.org/10.1130/g31352.1>, 2011.

881 Hilton, R. G., Galy, V., Gaillardet, J., Dellinger, M., Bryant, C., O'Regan, M., Grocke, D. R., Coxall, H., Bouchez, J.,  
882 and Calmels, D.: Erosion of organic carbon in the Arctic as a geological carbon dioxide sink, *Nature*, 524, 84–7,  
883 <https://doi.org/10.1038/nature14653>, 2015.

884 Hu, B., Li, J., Bi, N., Wang, H., Wei, H., Zhao, J., Xie, L., Zou, L., Cui, R., Li, S., Liu, M., and Li, G.: Effect of  
885 human-controlled hydrological regime on the source, transport, and flux of particulate organic carbon from the lower  
886 Huanghe (Yellow River), *Earth Surface Processes and Landforms*, 40, 1029–1042, <https://doi.org/10.1002/esp.3702>,  
887 2015.

888 Hua, Q., Barbetti, M., and Rakowski, A. Z.: Atmospheric Radiocarbon for the Period 1950–2010, *Radiocarbon*, 55,  
889 2059–2072, [https://doi.org/10.2458/azu\\_js\\_rc.v55i2.16177](https://doi.org/10.2458/azu_js_rc.v55i2.16177), 2013.

890 Huang, C. C., and Ren, Z.: Fluvial erosion and the formation of gully systems over the Chinese Loess Plateau, *WSEAS*  
891 *Transactions on Environment and Development*, 2(2), 141–145, 2006.

892 Jahn, B., Gallet, S., and Han, J.: Geochemistry of the Xining, Xifeng and Jixian sections, Loess Plateau of China:  
893 eolian dust provenance and paleosol evolution during the last 140 ka, *Chemical Geology*, 178, 71–94,  
894 [https://doi.org/10.1016/S0009-2541\(00\)00430-7](https://doi.org/10.1016/S0009-2541(00)00430-7), 2001.

895 Ke, Y., Calmels, D., Bouchez, J., and Quantin, C.: MODern River archivEs of Particulate Organic Carbon:  
896 MOREPOC, *Earth System Science Data Discussions*, 1–19, <https://doi.org/10.5194/essd-2022-161>, 2022.

897 Keil, R. G., Mayer, L. M., Quay, P. D., Richey, J. E., and Hedges, J. I.: Loss of organic matter from riverine particles  
898 in deltas, *Geochimica et Cosmochimica Acta*, 61, 1507–1511, [https://doi.org/10.1016/S0016-7037\(97\)00044-6](https://doi.org/10.1016/S0016-7037(97)00044-6), 1997.

899 Gen Li, X. T. W., Zhongfang Yang, Changping Mao, A. Joshua West, Junfeng Ji: Dam-triggered organic carbon  
900 sequestration makes the Changjiang (Yangtze) river basin (China) a significant carbon sink, *Journal of Geophysical*  
901 *Research: Biogeosciences*, 2015.

902 [Li, P., Chen, J., Zhao, G., Holden, J., Liu, B., Chan, F. K. S., Hu, J., Wu, P., and Mu, X.: Determining the drivers and  
903 rates of soil erosion on the Loess Plateau since 1901, \*Science of The Total Environment\*, 823, 153674,  
904 <https://doi.org/10.1016/j.scitotenv.2022.153674>, 2022.](https://doi.org/10.1016/j.scitotenv.2022.153674)

**Deleted:** Hatté, C., Tisnérat-Laborde, N., Ayrault, S., Balesdent, J., Chapon, V., Bourguignon, J., Alban, C., Ravel, S., Denax, L., Nguyen, C., Vavasseur, A., Sarrobert, C., Gasperi, J., Latrille, C., Savoye, S., Augusto, L., Conan Labbe, A., Bernard Michel, B., Douysset, G., Toqnelli, A., Vailhen, D., and Moulin, C.: Soil, climate and the environment - an indissociable threesome Soil carbon and global changes: reciprocal impacts; Carbon in all its forms; Echomicadas, a new tool to analyse carbon 14; Biotransformation of metallic trace elements by soil microorganisms; Absorption and distribution of metallic elements in plants; Dynamics of metallic contaminants in agricultural systems; Is photo-remediation for tomorrow? Hyper-accumulator plants; Sediments, tell me the Seine history The complex history of plant feeding by the soil; The environmental analysis, *Biofutur* (Paris), 26–57, 2016.

921 Licht, A., Pullen, A., Kapp, P., Abell, J., and Giesler, N.: Eolian cannibalism: Reworked loess and fluvial sediment as  
922 the main sources of the Chinese Loess Plateau, *GSA Bulletin*, 128, 944–956, <https://doi.org/10.1130/B31375.1>, 2016.

923 Liu, G., Xu, W., Zhang, Q., & Xia, Z.: Holocene Soil Chronofunctions, Luochuan, Chinese Loess Plateau.  
924 *Radiometric Dating*, 41, 2012.

925 Liu, J. and Liu, W.: Soil nitrogen isotopic composition of the Xifeng loess-paleosol sequence and its potential for use  
926 as a paleoenvironmental proxy, *Quaternary International*, 440, 35–41, <https://doi.org/10.1016/j.quaint.2016.04.018>,  
927 2017.

928 Liu, W., Yang, H., Ning, Y., and An, Z.: Contribution of inherent organic carbon to the bulk  $\delta^{13}\text{C}$  signal in loess  
929 deposits from the arid western Chinese Loess Plateau, *Organic Geochemistry*, 38, 1571–1579,  
930 <https://doi.org/10.1016/j.orggeochem.2007.05.004>, 2007.

931 Ludwig, W., Probst, J.-L., and Kempe, S.: Predicting the oceanic input of organic carbon by continental erosion,  
932 *Global Biogeochemical Cycles*, 10, 23–41, <https://doi.org/10.1029/95gb02925>, 1996.

933 Mayorga, E., Aufdenkampe, A. K., Masiello, C. A., Krusche, A. V., Hedges, J. I., Quay, P. D., Richey, J. E., and  
934 Brown, T. A.: Young organic matter as a source of carbon dioxide outgassing from Amazonian rivers, *Nature*, 436,  
935 538–41, <https://doi.org/10.1038/nature03880>, 2005.

936 Milliman, J. D. and Farnsworth, K. L.: *River discharge to the coastal ocean: a global synthesis*, Cambridge University  
937 Press, 2011.

938 Milliman, J. D., Yun-Shan, Q., Mei-E, R., and Saito, Y.: Man's Influence on the Erosion and Transport of Sediment  
939 by Asian Rivers: The Yellow River (Huanghe) Example, *The Journal of Geology*, 95, 751–762,  
940 <https://doi.org/10.1086/629175>, 1987.

941 Moodie, A. J., Nittrouer, J. A., Ma, H., Carlson, B. N., Wang, Y., Lamb, M. P., and Parker, G.: Suspended Sediment-  
942 Induced Stratification Inferred From Concentration and Velocity Profile Measurements in the Lower Yellow River,  
943 China, *Water Resources Research*, 58, e2020WR027192, <https://doi.org/10.1029/2020WR027192>, 2022.

944 Ning, Y., Liu, W., and An, Z.: Variation of soil  $\delta^{13}\text{C}$  values in Xifeng loess-paleosol sequence and its  
945 paleoenvironmental implication, *CHINESE SCI BULL*, 51, 1350–1354, <https://doi.org/10.1007/s11434-006-1350-7>,  
946 2006.

947 Pan, B., Pang, H., Gao, H., Garzanti, E., Zou, Y., Liu, X., Li, F., and Jia, Y.: Heavy-mineral analysis and provenance  
948 of Yellow River sediments around the China Loess Plateau, *Journal of Asian Earth Sciences*, 127, 1–11,  
949 <https://doi.org/10.1016/j.jseaes.2016.06.006>, 2016.

950 Qu, Y., Jin, Z., Wang, J., Wang, Y., Xiao, J., Gou, L.-F., Zhang, F., Liu, C.-Y., Gao, Y., Suarez, M. B., and Xu, X.:  
951 The sources and seasonal fluxes of particulate organic carbon in the Yellow River, *Earth Surface Processes and*  
952 *Landforms*, <https://doi.org/10.1002/esp.4861>, 2020.

953 Ran, L., Lu, X. X., and Xin, Z.: Erosion-induced massive organic carbon burial and carbon emission in the Yellow  
954 River basin, China, *Biogeosciences*, 11, 945–959, <https://doi.org/10.5194/bg-11-945-2014>, 2014.

955 Ran, L., Lu, X. X., Sun, H., Han, J., Li, R., and Zhang, J.: Spatial and seasonal variability of organic carbon transport  
956 in the Yellow River, China, *Journal of Hydrology*, 498, 76–88, <https://doi.org/10.1016/j.jhydrol.2013.06.018>, 2013.

957 Rao, Z., Guo, W., Cao, J., Shi, F., Jiang, H., and Li, C.: Relationship between the stable carbon isotopic composition  
958 of modern plants and surface soils and climate: A global review, *Earth-Science Reviews*, 165, 110–119,  
959 <https://doi.org/10.1016/j.earscirev.2016.12.007>, 2017.

960 Repasch, M., Scheingross, J. S., Hovius, N., Lupker, M., Wittmann, H., Haghypour, N., Gröcke, D. R., Orfeo, O.,  
961 Eglinton, T. I., and Sachse, D.: Fluvial organic carbon cycling regulated by sediment transit time and mineral  
962 protection, *Nat. Geosci.*, 14, 842–848, <https://doi.org/10.1038/s41561-021-00845-7>, 2021.

963 Rouse, H.: Modern Conceptions of the Mechanics of Fluid Turbulence, *Transactions of the American Society of Civil*  
964 *Engineers*, 102, 463–505, <https://doi.org/10.1061/TACEAT.0004872>, 1937.

965 Schwab, M. S., Hilton, R. G., Haghypour, N., Baronas, J. J., and Eglinton, T. I.: Vegetal Undercurrents—Obscured  
966 Riverine Dynamics of Plant Debris, *Journal of Geophysical Research: Biogeosciences*, 127, e2021JG006726,  
967 <https://doi.org/10.1029/2021JG006726>, 2022.

968 Shi, H. and Shao, M.: Soil and water loss from the Loess Plateau in China, *Journal of Arid Environments*, 45, 9–20,  
969 <https://doi.org/10.1006/jare.1999.0618>, 2000.

970 Stevens, T., Carter, A., Watson, T. P., Vermeesch, P., Andò, S., Bird, A. F., Lu, H., Garzanti, E., Cottam, M. A., and  
971 Sevastjanova, I.: Genetic linkage between the Yellow River, the Mu Us desert and the Chinese Loess Plateau,  
972 *Quaternary Science Reviews*, 78, 355–368, <https://doi.org/10.1016/j.quascirev.2012.11.032>, 2013.

973 Sun, D., Tang, J., He, Y., Liao, W., and Sun, Y.: Sources, distributions, and burial efficiency of terrigenous organic  
974 matter in surface sediments from the Yellow River mouth, northeast China, *Organic Geochemistry*, 118, 89–102,  
975 <https://doi.org/10.1016/j.orggeochem.2017.12.009>, 2018.

Formatted: Left, Pattern: Clear

Formatted: Font color: Auto, English (US)

Formatted: Normal, Left

Formatted: Font color: Auto, English (US)

976 Syvitski, J. P. M., Vörösmarty, C. J., Kettner, A. J., and Green, P.: Impact of Humans on the Flux of Terrestrial  
977 Sediment to the Global Coastal Ocean, *Science*, 308, 376–380, <https://doi.org/10.1126/science.1109454>, 2005.

978 Tao, S., Eglinton, T. I., Montluçon, D. B., McIntyre, C., and Zhao, M.: Pre-aged soil organic carbon as a major  
979 component of the Yellow River suspended load: Regional significance and global relevance, *Earth and Planetary  
980 Science Letters*, 414, 77–86, <https://doi.org/10.1016/j.epsl.2015.01.004>, 2015.

981 Tao, S., Eglinton, T. I., Montluçon, D. B., McIntyre, C., and Zhao, M.: Diverse origins and pre-depositional histories  
982 of organic matter in contemporary Chinese marginal sea sediments, *Geochimica et Cosmochimica Acta*, 191, 70–88,  
983 <https://doi.org/10.1016/j.gca.2016.07.019>, 2016.

984 Tao, S., Eglinton, T. I., Zhang, L., Yi, Z., Montluçon, D. B., McIntyre, C., Yu, M., and Zhao, M.: Temporal variability  
985 in composition and fluxes of Yellow River particulate organic matter, *Limnology and Oceanography*, 63, S119–S141,  
986 <https://doi.org/10.1002/lno.10727>, 2018.

987 [Turowski, J. M., Hilton, R. G., and Sparkes, R.: Decadal carbon discharge by a mountain stream is dominated by  
988 coarse organic matter, \*Geology\*, 44, 27–30, 2016.](https://doi.org/10.1016/j.geology.2016.07.019)

989 Walling, D. E. and Fang, D.: Recent trends in the suspended sediment loads of the world's rivers, *Global and Planetary  
990 Change*, 39, 111–126, [https://doi.org/10.1016/S0921-8181\(03\)00020-1](https://doi.org/10.1016/S0921-8181(03)00020-1), 2003.

991 Wang, C., Li, F., Shi, H., Jin, Z., Sun, X., Zhang, F., Wu, F., and Kan, S.: The significant role of inorganic matters in  
992 preservation and stability of soil organic carbon in the Baoji and Luochuan loess/paleosol profiles, Central China,  
993 *CATENA*, 109, 186–194, <https://doi.org/10.1016/j.catena.2013.04.001>, 2013.

994 Wang, G., Feng, X., Han, J., Zhou, L., Tan, W., and Su, F.: Paleovegetation reconstruction using  $\delta^{13}\text{C}$  of Soil Organic  
995 Matter, *Biogeosciences*, 5, 1325–1337, <https://doi.org/10.5194/bg-5-1325-2008>, 2008.

996 Wang, H., Bi, N., Saito, Y., Wang, Y., Sun, X., Zhang, J., and Yang, Z.: Recent changes in sediment delivery by the  
997 Huanghe (Yellow River) to the sea: Causes and environmental implications in its estuary, *Journal of Hydrology*, 391,  
998 302–313, <https://doi.org/10.1016/j.jhydrol.2010.07.030>, 2010.

999 Wang, H., Wu, X., Bi, N., Li, S., Yuan, P., Wang, A., Syvitski, J. P. M., Saito, Y., Yang, Z., Liu, S., and Nittrouer, J.:  
1000 Impacts of the dam-orientated water-sediment regulation scheme on the lower reaches and delta of the Yellow River  
1001 (Huanghe): A review, *Global and Planetary Change*, 157, 93–113, <https://doi.org/10.1016/j.gloplacha.2017.08.005>,  
1002 2017.

1003 Wang, H., Yang, Z., Saito, Y., Liu, J. P., Sun, X., and Wang, Y.: Stepwise decreases of the Huanghe (Yellow River)  
1004 sediment load (1950–2005): Impacts of climate change and human activities, *Global and Planetary Change*, 57, 331–  
1005 354, <https://doi.org/10.1016/j.gloplacha.2007.01.003>, 2007.

1006 Wang, S., Fu, B., Piao, S., Lü, Y., Ciais, P., Feng, X., and Wang, Y.: Reduced sediment transport in the Yellow River  
1007 due to anthropogenic changes, *Nature Geosci*, 9, 38–41, <https://doi.org/10.1038/ngeo2602>, 2016.

1008 Wang, X., Xu, C., Druffel, E. M., Xue, Y., and Qi, Y.: Two black carbon pools transported by the Changjiang and  
1009 Huanghe Rivers in China, *Global Biogeochemical Cycles*, 2016.

1010 Weiguo, L., Xiahong, F., Youfeng, N., Qingle, Z., Yunning, C., and Zhisheng, A. N.:  $\delta^{13}\text{C}$  variation of C3 and C4  
1011 plants across an Asian monsoon rainfall gradient in arid northwestern China, *Global Change Biology*, 11, 1094–1100,  
1012 <https://doi.org/10.1111/j.1365-2486.2005.00969.x>, 2005.

1013 Xiubin, H., Tang, K., and Zhang, X.: Soil Erosion Dynamics on the Chinese Loess Plateau in the Last 10,000 Years,  
1014 *Journal of Geology*, 24, 342–347, [https://doi.org/10.1659/0276-4741\(2004\)024\[0342:SEDOTC\]2.0.CO;2](https://doi.org/10.1659/0276-4741(2004)024[0342:SEDOTC]2.0.CO;2), 2004.

1015 [Xue, D., Lu, J., Leung, L. R., Teng, H., Song, F., Zhou, T., and Zhang, Y.: Robust projection of East Asian summer  
1016 monsoon rainfall based on dynamical modes of variability, \*Nat Commun\*, 14, 3856, \[https://doi.org/10.1038/s41467-  
1017 023-39460-y\]\(https://doi.org/10.1038/s41467-023-39460-y\), 2023.](https://doi.org/10.1038/s41467-023-39460-y)

1018 [YRCC \(Yellow River Conservation Committee\): Annual Sediment Report for the Yellow River, 2016.](https://doi.org/10.1016/j.gloplacha.2016.07.019)

1019 Yu, M., Eglinton, T. I., Haghypour, N., Montluçon, D. B., Wacker, L., Hou, P., Zhang, H., and Zhao, M.: Impacts of  
1020 Natural and Human-Induced Hydrological Variability on Particulate Organic Carbon Dynamics in the Yellow River,  
1021 *Environ Sci Technol*, 53, 1119–1129, <https://doi.org/10.1021/acs.est.8b04705>, 2019a.

1022 Yu, M., Eglinton, T. I., Haghypour, N., Montluçon, D. B., Wacker, L., Wang, Z., Jin, G., and Zhao, M.: Molecular  
1023 isotopic insights into hydrodynamic controls on fluvial suspended particulate organic matter transport, *Geochimica et  
1024 Cosmochimica Acta*, 262, 78–91, <https://doi.org/10.1016/j.gca.2019.07.040>, 2019b.

1025 Zhang, L. J., Wang, L., Cai, W. J., Liu, D. M., and Yu, Z. G.: Impact of human activities on organic carbon transport  
1026 in the Yellow River, *Biogeosciences*, 10, 2513–2524, <https://doi.org/10.5194/bg-10-2513-2013>, 2013.

1027 Zhu, T. X.: Gully and tunnel erosion in the hilly Loess Plateau region, China, *Geomorphology*, 153–154, 144–155,  
1028 <https://doi.org/10.1016/j.geomorph.2012.02.019>, 2012.

Formatted: English (US)